Manuscript prepared for Earth Syst. Dynam.
with version 2014/07/29 7.12 Copernicus papers of the LaTeX class copernicus.cls.
Date: 11 February 2015

The impact of oceanic heat transport on the atmospheric circulation

M.-A. Knietzsch[1], A. Schröder[1], V. Lucarini[1,2], and F. Lunkeit[1]

[1]Meteorologisches Institut, Universität Hamburg, Hamburg, Germany
[2]Department of Mathematics and Statistics, University of Reading, Reading, UK

Correspondence to: F. Lunkeit (frank.lunkeit@uni-hamburg.de)

Abstract. A general circulation model of intermediate complexity with an idealized earth–like aqua-planet setup is used to study the impact of changes in the oceanic heat transport on the global atmospheric circulation. Focus is put on the atmospheric mean meridional circulation and global thermodynamic properties.

The atmospheric heat transport compensates the imposed oceanic heat transport changes to a large extent in conjunction with significant modification of the general circulation. Up to a maximum about 3 PW, an increase of the oceanic heat transport leads to an increase of the global mean near–surface temperature and a decrease of its equator–to–pole gradient. For larger transports, the gradient is reduced further but the global mean remains approximately constant. This is linked to a cooling and a reversal of the temperature gradient in the tropics.

Both the Hadley and Ferrel cell show a decline for increasing oceanic heat transport and poleward shift of their maxima. Changes in zonal mean diabatic heating and ~~in the~~ friction impact the properties of the Hadley cell, while the behavior of the Ferrell cell is mostly controlled by friction. Changes in atmospheric heat transport are related to the strength of the residual mean circulation where eddy transport of heat is the most important source.

The efficiency of the climate machine, the intensity of the Lorenz energy cycle and the material entropy production of the system decline with increased oceanic heat transport. This suggests that the climate system becomes less efficient and turns into a state of reduced entropy production, as the enhanced oceanic transport performs a stronger large–scale mixing between geophysical fluids with different temperature, thus reducing the availability in the climate system and bringing it closer to a state of thermal equilibrium.

1 Introduction

The climate is a forced and dissipative non–equilibrium system, which - neglecting secular trends - can be considered in steady state, i.e. its statistical properties do not depend on time. Astronomical factors and differences of local albedo cause a difference of net incoming shortwave radiation between low and high latitudes leading to differential heating and a surplus of energy in the tropics. Considering global and long–term averages the same amount of supplied energy is emitted to space, so that the incoming shortwave radiation is balanced by the outgoing longwave radiation (Peixoto and Oort, 1992; Lucarini and Ragone, 2011). The ocean and atmosphere transport the excess of energy from the tropics to high latitudes.

The oceanic and atmospheric ~~transport results~~ from the conversion of available potential energy - due to the inhomogeneous absorption of solar radiation, with positive correlation between heating and temperature patterns - into kinetic energy, through instabilities ~~coming~~, typically, from the presence of temperature gradients (Lorenz, 1955). Such instabilities tend to reduce the same temperature gradients they feed upon by mixing oceanic and atmospheric masses. The kinetic energy is then dissipated inside the system. The production of available potential energy, its conversion to kinetic energy, and the dissipation of kinetic energy have the same average rate, which corresponds to the intensity of the Lorenz (1955; 1967) energy cycle.

Recently, using tools of macroscopic non–equilibrium thermodynamics, a line has been drawn connecting a measure of the efficiency of the climate system, the spatio–temporal variability of its heating and temperature fields, the intensity of the Lorenz energy cycle and the material entropy production (Johnson, 2000; Lucarini, 2009; Lucarini et al., 2011). As mentioned above, the climate can be considered as a (forced and dissipative) non–equilibrium thermodynamic system where the entropy budget is achieved in such a way that the sum of the integrated incoming entropy flux due to the solar high frequency photons, and the entropy generated by irreversible processes in the atmosphere and ocean, is compensated by the radiation to space of low frequency photons. Most of the entropy production results from optical processes, while a smaller portion - referred to as material entropy production - is related to the irreversible processes in terms of the geophysical fluids (Kleidon and Lorenz, 2005). So the Earth is, in contrast to a system that is isolated and therefore ~~maintaining~~ a state of equilibrium, a thermodynamic system that exchanges energy and entropy with space (Ambaum, 2010).

Stone (1978) argued that the magnitude of the total meridional heat transport, i.e. the sum of the oceanic and the atmospheric contributions, is insensitive to the structure and the specific dynamical properties of the atmosphere–ocean system, so that changes of the oceanic heat transport (OHT) will be compensated by the atmospheric flow and vice versa. In particular, he suggested that the peak of the heat transport is constrained within a narrow range of latitudes regardless of the radiative forcing. The features of the meridional heat transport can be related to the solar constant, the radius of the Earth, the tilt of the Earth's axis and the hemispheric mean albedo. Stone argued that the

insensitivity to the structure and the dynamics of the system is due to the correlation of thermal emissions to space, the albedo and the efficiency of the transport mechanisms of the atmosphere and the ocean.

Enderton and Marshall (2008) discussed the limits of Stone's hypothesis by employing a series of coupled atmosphere–ocean–sea–ice model experiments in which the oceanic circulation on an aqua-planet is constrained by different meridional barriers. The presence or absence of the barriers result in significantly different climates, in particular in climates with and without polar ice caps. They concluded that Stone's result is a good guide for ice–free climates. But, if polar ice caps are present, the effect of the related meridional gradients in albedo on the absorption of solar radiation need to be taken into account.

The atmospheric compensation implies a significant impact of changes in OHT on the atmospheric circulation as a whole which affects the zonally symmetric flow, the zonally asymmetric (eddy) flow and the interplay between both. Thus, changes in OHT have been commonly used to account for paleo–climatic changes (e.g. Rind and Chandler, 1991; Sloan et al., 2001; Romanova et al., 2006). Moreover, OHT is an important factor for potential anthropogenic climate change since significant modifications of it can be expected. Unfortunately, there are large uncertainties in the changes in the oceanic circulation simulated in climate change scenarios (IPCC, 2013). These result from, amongst others, ~~the~~ uncertainties in fresh water forcing due to potential melting of inland ice sheets. To assess the role of the ocean for historical and potential future climates the impact of the OHT on the atmospheric circulation and the underlying mechanisms need to be investigated systematically.

A way of studying the impact of changes in OHT on the atmospheric circulation is to utilize an atmospheric general circulation model coupled to a mixed–layer ocean. In such a model the OHT can be prescribed. Using a present–day setup including continents Winton (2003), Herweijer et al. (2005), and Barreiro et al. (2011) found that increasing OHT results in a warmer climate with less sea–ice. A reduction of low–level clouds and an increase of greenhouse trapping due to a moistening of the atmosphere appeared to be relevant mechanisms. In addition, a weakening of the Hadley cell with increased OHT was found by Herweijer et al. (2005) and Barreiro et al. (2011).

Utilizing an idealized aqua–planet setup Rose and Ferreira (2013) systematically assessed the impact of the OHT on the atmospheric global mean near–surface temperature and its equator–to–pole gradient. For warm and ice–free climates they confirm a near–perfect atmospheric compensation of the imposed changes in OHT. Like in the above studies including continents, they found an increase in global mean temperature for increasing OHT, accompanied by a decrease in the equator–to–pole temperature gradient. Tropical SSTs were shown to be less affected than at higher latitudes. The detailed meridional structure of the oceanic heat transport turned out to be less important. Changes in deep moist convection in the mid–latitudes, together with an enhanced water vapor greenhouse appear to be the major drivers. Koll and Abbot (2013) confirmed the low sensitivity of tropical SSTs to OHT changes. In their aqua–planet experiments, larger OHT leads to a weakening of the

Hadley cell which reduces cloud cover and surface winds, and thus, counteracts surface cooling by increasing OHT.

In the present study we extend and supplement the above studies. Based on the experimental setup of Rose and Ferreira (2013) we focus on the impact of OHT changes on the atmospheric dynamics and thermodynamics. Our overall goal is to understand how the atmospheric energy transport and transformations are affected by modulations in the oceanic oceanic transport. We analyse the changes in the atmospheric heat transport and the mean meridional circulation by employing, amongst others, the Kuo–Eliassen equation (Kuo, 1956; Eliassen, 1951) in order to understand the various drivers of the mean meridional circulation. Furthermore, the integrated effect on the atmospheric energetics is assessed by means of the Lorenz energy cycle and by changes in the properties of the effective warm and cold reservoirs constructed according to the theory proposed in Johnson (2000) and Lucarini (2009). This allows for defining a measure of the efficiency of the climate system. Attention is directed to measuring the irreversibility of the atmosphere and the material entropy production. This part tries to frame specific climatic processes of general relevance into a general physical framework, trying to advance the understanding of the climate as a non–equilibrium, forced and dissipative macroscopic system.

The paper is organized as follows. In Sect. 2 we describe the model and the experimental design. Sect. 3 introduces our diagnostics. The results of the analyses are presented in Sect. 4. A summary and discussion concludes the paper (Sect. 5).

2 Model and experimental setup

The Planet Simulator (PlaSim, http://www.mi.uni-hamburg.de/Planet-Simul.216.0.html) is an open source general circulation model (GCM) of intermediate complexity developed at the University of Hamburg. For the atmosphere, the dynamical core is the Portable University Model of the Atmosphere (PUMA) based on the primitive equation multi–level spectral model of Hoskins and Simmons (1975) and James and Gray (1986). Radiation is parameterized by differentiating between shortwave and longwave radiation and between a clear or a cloudy atmosphere. The respective schemes follow the works of Lacis and Hansen (1974) for the short wave part and Sasamori (1968) for the long–wave part. The radiative properties of clouds based on Stephens (1978) and Stephens et al. (1984). Cloud fraction is computed according to Slingo and Slingo (1991). The representation of boundary–layer fluxes and of vertical and horizontal diffusion follows Louis (1979), Louis et al. (1982), Roeckner et al. (1992), and Laursen and Eliasen (1989). The cumulus convection scheme is based on Kuo (1965, 1974). The ocean is represented by a thermodynamic mixed–layer (slab ocean) model including a one layer thermodynamic sea–ice component.

Following Rose and Ferreira (2013) we used an earthlike aqua-planet setup with zonally symmetric forcing utilizing reference present day conditions for the solar constant ($1365\,\mathrm{W\,m^{-2}}$)

and the CO_2-concentration ($360\,\mathrm{ppm}$). The solar insolation comprises an annual cycle (with obliquity=23.4°) but eccentricity is set to zero. Thus, on annual average the forcing is hemispherically symmetric as well. The mixed–layer depth is set to 60 m.

A temporally constant flux into the ocean (q–flux) is used to prescribe the oceanic heat transport (OHT) according to the analytic equation given by Rose and Ferreira (2013):

$$\mathrm{OHT} = \mathrm{OHT}_0 \cdot \sin(\phi)\cos(\phi)^{2N} \tag{1}$$

where ϕ denotes the latitude. N is a positive integer which determines the latitude of the maximum of the transport and the shape of its meridional profile, and OHT_0 is a constant defining the magnitude. Rose and Ferreira made sensitivity experiments by varying N (ranging from 1 to 8) and by varying the peak transport (ranging from 0 to 4 PW) which is controlled by OHT_0.

For our study we follow Rose and Ferreira but fix the location of the peak by setting $N = 2$ (which corresponds to maximum transport at 27°). We perform nine sensitivity simulations with respect to the magnitude of the transport by changing OHT_0 to obtain peak transports $\mathrm{OHT}_{\mathrm{max}}$ from 0 PW to 4 PW (with 0.5 PW increment). $\mathrm{OHT}_{\mathrm{max}} = 0$ PW (i.e. no OHT) serves as the control simulation. The OHT for $\mathrm{OHT}_{\mathrm{max}} = 0$, 1, 2, 3 and 4 PW is displayed in Fig. 1.

All simulations are run for at least 100 years (360 days per year). The last 30 years are subject to the analyses. A horizontal resolution of $T31$ (96×48 grid points) with five σ–levels in the vertical is used. The timestep is $\Delta t = 23$ min.

3 Diagnostics

The dominant feature of the large scale ocean and the atmosphere dynamics is the transport of energy from regions featuring net positive energy budget at the top of the atmosphere low latitudes) to regions where such budget is negative (high latitudes). This reduces the temperature gradient between equator and poles (e.g. Peixoto and Oort, 1992; Lucarini and Ragone, 2011). In present conditions, The partitioning of heat transport between atmosphere and ocean reflects two limits: the dominance of the atmospheric mass transport in mid–to–high latitudes and the dominance of the oceanic energy transport in the tropics. The atmospheric transport can be further subdivided in the sensible heat, latent heat and potential energy components. We will investigate the response of changes in the imposed OHT for each of these components, and will further specify the analysis by considering both the zonally symmetric contributions, due to the mean meridional circulation (MMC) and the zonally asymmetric contributions, due to the atmospheric eddies.

In the classical view (the Eulerian mean circulation), the mean meridional circulation consists of three cells: the tropical Hadley cell, the Ferrel cell in mid–latitudes and a weak polar cell. While the Hadley and the polar cell are thermally direct circulations, i.e. relatively warm air is rising and cold air is sinking, the Ferrel cell is referred to as a thermally indirect cell with warm air sinking and cold air rising. Though the mean meridional circulation can be viewed as a two dimensional circulation in

the meridional–height plane, both zonally symmetric and zonally asymmetric components contribute to its existence.

The transformed Eulerian mean (TEM) formalism (Andrews and McIntyre 1976) accounts for the role of the eddies in the mean meridional transport. In particular, it provides a closer link to the total atmospheric meridional heat transport. The TEM residual circulation approximates the isentropic mean circulation resulting in a single cell from the equator to the pole. Based on work by Held (2001), Czaja and Marshall (2006) showed that the atmospheric heat transport can be represented by the product of the strength of the TEM residual circulation and the vertical energy contrast.

Utilizing the Kuo–Eliassen equations allows to identify individual drivers of the Eulerian mean meridional circulation (Appendix A). A similar partitioning is done for TEM residual steamfunction which provides a direct link to the atmospheric heat transport. This summarizes the diagnostics tools aimed at capturing a phenomenological description of the atmospheric circulation.

A second set of diagnostic tools is based on taking a thermodynamical point of view on the atmospheric circulation. One finds that on the average a net positive work resulting from the positive correlation between temperature and heating fields upholds the kinetic energy of the global circulation against the frictional dissipation (Peixoto and Oort, 1992).

The atmospheric energy cycle (Lorenz, 1955, 1967) is one of the most important concepts to understand the global atmospheric circulation as it provides a comprehensive look at the integrated effects of physical mechanisms involved, the generation of available potential energy by external forcing, the dissipation of kinetic energy and the energy conversions by baroclinic and barotropic processes. If the climate system is ~~at~~ statistical steady state, the rate of generation of available potential energy $\dot{G}$, the rate of conversion of potential into kinetic energy $\dot{W}$, and the dissipation rate of kinetic energy $\dot{D}$ are equal when averaged over a long period of time (e.g. several years). Thus, $\overline{\dot{G}} = \overline{\dot{W}} = \overline{\dot{D}} > 0$, where the bar indicates the operation of time averaging. This allows for characterizing the strength of the energy cycle in several ways.

Following the work by Johnson (2000) and Lucarini (2009) we consider the global energy cycle as resulting from the work of an equivalent Carnot engine operating between the two (dynamically determined) reservoirs at temperature Θ^+ and Θ^-. According to this concept, an efficiency of the climate system (η) can be defined by

$$\eta = \frac{\Theta^+ - \Theta^-}{\Theta^+} \tag{2}$$

Furthermore, following the same theoretical point of view we analyse the entropy production which leads to a measure of the irreversibility. An outline of the theory and the according diagnostics is given in Appendix B.

The diagnostics of Lorenz' formulation of the energy cycle reveals information about the reservoirs partitioned into zonal mean and eddy components, and about the conversions due to different

physical processes (Appendix C). Thus, we gain evidence about the relative importance of the individual components contributing to the energy cycle and the related thermodynamic properties.

4 Results

4.1 Atmospheric dynamics

We start presenting the effect of OHT changes on the mean climate in terms of atmospheric near–surface (2m) temperature, sea–ice and meridional heat transport. First, we note that similar to Rose and Ferreira (2013) our model exhibits multiple equilibria, a warm state and a snow–ball Earth depending on the initial conditions as thoroughly discussed in Boschi et al. (2012) and Lucarini et al. (2013). In the present study we investigate the warm states only. However, in contrast to Rose and Ferreira (2013) sea–ice at high latitudes is present in all of the warm state simulations.

Up to about $\mathrm{OHT}_{\mathrm{max}} = 2.5\,\mathrm{PW}$ increasing OHT leads to an increase of the global mean (T_{M}) and a decrease of the equator–to–pole gradient (ΔT) of the annual and zonal mean near-surface air temperature (Fig. 2). For this regime an approximately linear relationship between T_{Mean} and ΔT can be found. For $\mathrm{OHT}_{\mathrm{max}} > 2.5\,\mathrm{PW}$, T_{M} is almost insensitive to an OHT change while ΔT is further reduced. Here, the equator–to–pole gradient is defined by the difference between the values at the lowest and highest latitude of the model's grid.

When inspecting the respective meridional profiles of the annual and zonal mean near–surface temperatures, we observe that high latitudes are more sensitive to the OHT changes than low latitudes. With increasing OHT, the polar temperatures continuously increase except for $\mathrm{OHT}_{\mathrm{max}} = 4\,\mathrm{PW}$ where slightly colder polar temperatures than for $\mathrm{OHT}_{\mathrm{max}} = 3.5\,\mathrm{PW}$ are found. It appears that this is a consequence of the reduced atmospheric heat transport, slightly over–compensating the increased but still small oceanic heat transport at these latitudes (see later discussion). In the tropics, an increase of the temperatures is only present until $\mathrm{OHT}_{\mathrm{max}} = 1.5\,\mathrm{PW}$. For larger OHT, the equatorial temperatures decrease. In addition, increasing OHT leads to a flattening of the temperature profile in the tropics until, for $\mathrm{OHT}_{\mathrm{max}} = 3.5$ and 4 PW, the temperature gradient in the tropics gets reversed and the maximum of the temperature shifts away from the equator to approx. $\pm 24°$.

Sea–ice gradually decreases with increasing OHT. But, even for $\mathrm{OHT}_{\mathrm{max}} = 4\,\mathrm{PW}$ some sea–ice remains in polar latitudes. However, for $\mathrm{OHT}_{\mathrm{max}} > 2\,\mathrm{PW}$ the average sea–ice cover is smaller than 1 indicating that no latitude is completely covered by sea–ice during the whole year.

Qualitatively, all findings are also true for winter and summer as can be seen in Fig. 3, except that in summer the sensitivity to OHT changes is small ~~in~~ the high latitudes ~~which~~ are covered by sea–ice. In addition, we note that the seasonality and its sensitivity to OHT changes are small for latitudes without sea–ice due to the high thermal inertia of the mixed–layer. In the following we restrict the analysis to the annual mean.

Despite the difference in sea–ice extent (i.e. planetary albedo), the atmospheric heat transport compensates the changes in OHT to a ~~great~~ extent, as can be seen from the total meridional heat transport diagnosed from the energy budget at the top of the atmosphere (Fig. 4). Figure 5 shows the annual mean zonally averaged atmospheric meridional heat transport for $\mathrm{OHT}_{\mathrm{max}} = 0, 1, 2, 3$ and 4 PW. We display the total transport and its components: the transport of sensible heat, latent heat and potential energy. In addition, we split each transport into the contribution from the zonally symmetric (zonal mean flow) and the asymmetric (eddy) part. For the total transport, the compensation for increasing OHT leads to a decrease of the atmospheric transport and a poleward shift of its maximum according to the prescribed OHT profile. Although the OHT is zonally symmetric, both atmospheric zonal mean flow and atmospheric eddies contribute to the compensation.

In the tropics (0–30°), both the zonal mean flow and the eddies account for the atmospheric transport, with the eddy component being dominant in the outer tropics, where the zonal mean flow contribution decreases to zero. For the eddy transport in the tropics, only the latent heat transport is relevant ~~f~~. For the zonal mean flow, the magnitude of all three components decrease with increasing OHT showing about the same relative change per 1 PW $\mathrm{OHT}_{\mathrm{max}}$. The total mean flow transport, however, ~~results from~~ a large compensation of equatorward sensible and latent heat transport (of approx. same order of magnitude) and poleward transport of potential energy.

In ~~the~~ mid–latitudes, ~~the~~ eddies dominate the poleward heat transport and its sensitivity to OHT changes, with the contribution from latent heat transport being concentrated equatorward of ~~that~~ from sensible heat transport. Transport of potential energy by eddies is almost absent due to their geostrophic nature.

In summary, the atmospheric compensation for changes in OHT takes place according to the relative importance of the respective component for the transport in the reference state where no OHT is present. Although ~~the~~ changes in OHT are very large it appears that the role of the different processes in controlling the total heat transport remains unchanged.

We next study the atmospheric mean meridional circulation starting with the classical Eulerian mean circulation described by mass streamfunction ψ. Figure 6 shows Northern Hemisphere ψ for $\mathrm{OHT}_{\mathrm{max}} = 0$, 2, 3 and 4 PW. For $\mathrm{OHT}_{\mathrm{max}} = 0$ PW, a Hadley cell and a Ferrel cell are well established with values of about 8×10^{10} and $-3 \times 10^{10}\,\mathrm{kg\,s^{-1}}$, respectively. The maximum magnitudes are located at about 10° N for the Hadley cell and 50° N for the Ferrel cell, and at about 700 hPa for both cells. The Hadley cell extends to about 33° N. A polar cell is absent in the annual mean but emerges weakly in the summer months.

With increasing OHT, the strength of both cells decreases (Fig. 7). The decrease in strength of the Hadley cell is virtually linear and amounts to about 85 %. The Ferrel cell strength decreases by about 50 % with stronger decreases for smaller $\mathrm{OHT}_{\mathrm{max}}$. The Ferrel cell shifts poleward. For $\mathrm{OHT}_{\mathrm{max}} > 2$ PW, a poleward shift can also be observed for the Hadley cells maximum together with a broadening of this cell, i.e. a poleward shift of its edge. For $\mathrm{OHT}_{\mathrm{max}} = 4$ PW, an additional

thermally indirect cell can be observed close to the equator. This is related to an almost vanished Hadley cell in summer together with a winter hemisphere Hadley cell which has its maximum on the summer hemisphere.

The Kuo–Eliassen equation allows for identifying individual drivers of the Eulerian mean meridional circulation (Appendix A). The reconstructions by means of the Kuo–Eliassen equation are in good agreement with the actual ψ for all simulations. However, the maximum magnitudes are systematically overestimated. In general, the reconstruction ~~fits better,~~ for the Hadley cell than for the Ferrel cell (Fig. 9).

As an example, Figure 8 shows the sources and the reconstruction for $\mathrm{OHT}_{\mathrm{max}} = 0\,\mathrm{PW}$. The individual sources indicate that the largest contributions to ψ stem from diabatic heating and from friction. The heating controls the Hadley cell together with a significant contribution by friction. For the Ferrel cell, friction is the most important factor. To a much smaller extent, ~~the~~ eddy transports of heat and ~~of~~ momentum add to the Ferrel circulation with a larger contribution by the heat transport. For both Hadley and Ferrel cell, the maximum contribution by friction is located at lower levels than for all other sources.

For the Hadley cell, both the contributions coming from heating and friction, decrease linearly with increasing OHT (Fig. 9). As the decrease is stronger for heating, friction becomes the major contributors to the Hadley cell for $\mathrm{OHT}_{\mathrm{max}} > 3\,\mathrm{PW}$. The decrease of the Ferrel cell with increasing OHT is linked to a decrease of the friction, i.e. a decrease of the near–surface zonal mean zonal wind. The contributions from ~~the~~ heat and momentum transports decrease less intensely than for the Hadley cell, and remain constant for $\mathrm{OHT}_{\mathrm{max}} > 2\,\mathrm{PW}$. Similar to ~~the~~ changes ~~of~~ magnitude, the shifting of the cells and the broadening of the Hadley cell can be explained by respective changes in the mean sources.

As pointed out by Czaja and Marshall (2006), the residual mean streamfunction ψ_{res} resulting from the transform Eulerian mean (TEM) formalism provides a much closer link between the meridional circulation and the atmospheric heat transport. In addition, it clarifies the role of the eddies for the transport. As shown in Appendix A a decomposition of ψ_{res} is possible similar to the Kuo–Eliassen equation. Here, the combined effect of the eddy momentum and the eddy heat transport is given in terms of the divergence of the Eliassen–Palm flux while the sources from diabatic heating and friction remain the same as in the Kuo–Eliassen case. We note that splitting the Eliassen–Palm flux into its components would result into the same contribution by the momentum transport for both the Eulerian mean and the TEM formulation.

Figure 10 gives the residual mean streamfunction, its reconstruction and the eddy source for $\mathrm{OHT}_{\mathrm{max}} = 0\,\mathrm{PW}$. Both the dry case and the moist case are presented. In the dry case, the eddy transport only concerns the dry static energy while in the moist case the transport of moist static energy is considered. As for the Eulerian mean, the reconstructions are in good agreement with the actual values (which again holds for all OHTs). Compared to the Eulerian mean (Figure 8) the residual

streamfunction displays a single overturning circulation with rising motion in the tropics and sinking air in high latitudes. While the maximum of the residual streamfunction occurs in mid–latitudes near the surface, a secondary maximum in the tropics is present in the dry case related to the Eulerian mean Hadley cell. From the reconstruction we see the dominance of the eddies for the mid–latitudes compared to the Eulerian mean case. Since the contribution from the eddy momentum transport is the same in the Eulerian mean and the TEM case, the differences are due to the heat transport only.

For all simulation, the residual mean circulation shows ~~the~~ one cell structure with maximum in ~~the~~ mid–latitudes close to the surface which is almost completely defined by the eddy source. For $\mathrm{OHT}_{\mathrm{max}} > 3\,\mathrm{PW}$ the secondary maximum in the tropics (dry case) disappears. With increasing OHT the strength of the circulation decreases. Figure 11 shows the meridional profile of maximum of the moist case residual streamfunction for $\mathrm{OHT}_{\mathrm{max}} = 0$, 1,2,3 and 4 PW. A comparison with the total atmospheric heat transport (Fig. 5) shows a good qualitative agreement, that is a decrease and a poleward shift of the maximum. An exception occurs for $\mathrm{OHT}_{\mathrm{max}} = 0\,\mathrm{PW}$ where the ψ_{res} maximum in located at about 50° while the heat transport peaks at about 35°. This is possibly caused by using pressure levels for the diagnostics introducing uncertainties close to the surface.

Based on work by Held (2001), Cazja and Marshall (2006) showed that the atmospheric heat transport can be represented by the product of the strength of the TEM residual circulation and the vertical difference in moist static energy. In agreement to this, a closer inspection of our results show that the relative decrease in ψ_{res} is smaller than the relative decrease in the heat transport. This difference can be explained by the decrease of the atmospheric stability (i.e. contrast in moist static energy) in mid–latitudes with increasing OHT (not shown).

4.2 Atmospheric thermodynamics

Now we shift our attention to the global thermodynamic properties and start with discussing Θ^+ and Θ^-, which characterize the warm and cold reservoirs of the climate engine. Such reservoirs are constructed in such a way to substantiate the fact that heating and temperature fields are positively correlated (See Appendix B). Qualitatively, the two temperatures behave similarly when $\mathrm{OHT}_{\mathrm{max}}$ is changed (Figure 12). We can classify three temperature regimes: i) $\mathrm{OHT}_{\mathrm{max}} < 2.0\,\mathrm{PW}$ atmospheric warming, ii) $2.0\,\mathrm{PW} \leq \mathrm{OHT}_{\mathrm{max}} \leq 3.5\,\mathrm{PW}$ atmospheric cooling, and iii) $\mathrm{OHT}_{\mathrm{max}} > 3.5\,\mathrm{PW}$ weak sensitivity. We observe a higher sensitivity of Θ^- than Θ^+ for i) which is generally due to the amplified polar warming. The difference between Θ^+ and Θ^-, denoted as $\Delta\Theta$, decreases with increasing $\mathrm{OHT}_{\mathrm{max}}$ implying a decrease in the atmospheric efficiency of the climate engine (see eq. 2). Interestingly, the difference between T_s and the average of Θ^- and Θ^+ increases with $\mathrm{OHT}_{\mathrm{max}}$, especially for $\mathrm{OHT}_{\mathrm{max}} \leq 3.0\,\mathrm{PW}$, indicating a reduction in the stability of the atmosphere. This is understood by considering that larger oceanic transports lead to stronger warming at low levels in the mid and high latitudes, which must be compensated by a weaker heat transport aloft.

The diabatic heating processes constitute the sources and sinks of internal energy for the atmosphere and play a decisive role in the generation and destruction of available potential energy (Peixoto and Oort, 1992). Those processes are displayed as the time– and zonal–averaged diabatic heating rates dT_a/dt (see figure 13). The heating rate is calculated as the sum over all diabatic heating effects including heating or cooling by the response of radiative heat fluxes, sensible and latent heat fluxes and vertical diffusion. While Θ^+ and Θ^- are defined using the time and space dependent heating fields, inspecting the time and zonal averages of the heating patterns is useful for understanding how available potential energy is generated (Lucarini et al., 2010).

Simulations with $0.5\,\mathrm{PW} \leq \mathrm{OHT_{max}} \leq 1.5\,\mathrm{PW}$ show diabatic warming in the deep tropics in the mid troposphere and in the subtropical low troposphere, whereas diabatic cooling occurs in the mid and high troposphere of the subtropics and in polar as well as subpolar regions. Positive heating in the tropical and subtropical regions is dominated by the contribution of latent heat fluxes, in particular, heating through convective precipitation (not shown here). In the mid to high latitude regions large–scale precipitation contributes towards a positive heating. Diabatic cooling, on the other hand, is mostly caused by outgoing longwave radiation and to a moderate extent by the conversion process from rain to snow mostly in the subtropical regions.

We see an extension of the area of positive heating in the mid latitudes towards the poles in the lower troposphere as well as in the equatorial mid and upper troposphere for larger values of $\mathrm{OHT_{max}}$. The poleward migration of the positive heating pattern in the mid–latitudes is closely related to the poleward shift of the atmospheric latent heat transport. The area of positive heating broadens in height at latitudes around $50°$. Since the positive heating patterns (relevant for defining Θ^+) in the mid latitudes extend in height and is, in addition, stretched poleward, lower temperatures are considered in the quantity of Θ^+, which explains the smaller sensitivity of Θ^+ than of Θ^- for $0\,\mathrm{PW} \leq \mathrm{OHT_{max}} \leq 1.5\,\mathrm{PW}$ in ~~figure~~ 12. By implication, the warming effect at polar latitudes causes the sensitivity of Θ^- to be larger than of Θ^+. For $\mathrm{OHT_{max}} \geq 2\,\mathrm{PW}$ the sensitivity of both, Θ^+ and Θ^-, is negative since large parts of the tropical high and mid troposphere cools.

We observe on average a decline in $\Delta\Theta$ of approximately $0.4\,\mathrm{K}$ for every $0.5\,\mathrm{PW}$ increase in $\mathrm{OHT_{max}}$ (figure 14; green graph). The total temperature difference decreases from $7.9\,\mathrm{K}$ to $4.5\,\mathrm{K}$ across the considered range of values of $\mathrm{OHT_{max}}$. The climate system becomes horizontally more isothermal as $\mathrm{OHT_{max}}$ is reinforced, which is consistent with the decline for the meridional difference in surface temperature $\Delta T = T_{s,eq} - T_{s,pole}$ (figure 14; blue graph). We find an accurate linear relation between ΔT and $\Delta\Theta$ (the temperature difference between the two thermal reservoirs, Θ^- and Θ^+): ~~for~~ every observed $10\,\mathrm{K}$ decline in ΔT the temperature difference, $\Delta\Theta$, decreases linearly by approximately $0.8\,\mathrm{K}$ on average, as shown in figure 14. This provides a potentially interesting indication of how to relate changes in the surface temperature gradient to quantities describing the dynamic processes in the atmosphere.

As the climate warms and the temperature difference between the warm and the cold reservoir shrinks with increased $\mathrm{OHT}_{\mathrm{max}}$, the efficiency η and the intensity of the Lorenz energy cycle $\overline{\dot{W}}$ of the climate system decline (see figure 15). The increase in $\mathrm{OHT}_{\mathrm{max}}$ causes the climatic machine to act less efficiently, in terms of a decrease of the ratio between mechanical energy output and thermal energy input.

We observe a remarkably linear behaviour for η and $\overline{\dot{W}}$ for $0\,\mathrm{PW} \leq \mathrm{OHT}_{\mathrm{max}} \leq 2.5\,\mathrm{PW}$ (Figure 15). For every $0.5\,\mathrm{PW}$ increase in $\mathrm{OHT}_{\mathrm{max}}$ the efficiency η declines by about $2.0 \cdot 10^{-3}$, while the strength of Lorenz energy cycle $\overline{\dot{W}}$ decreases by about $0.2\,\mathrm{Wm}^{-2}$ (see dotted, blue graph in figure 15). For $\mathrm{OHT}_{\mathrm{max}}$ larger than present–day values ($\mathrm{OHT}_{\mathrm{max}} \leq 2.5\,\mathrm{PW}$), η decreases by only $0.5 \cdot 10^{-3}$ per $0.5\,\mathrm{PW}$ increase, while $\overline{\dot{W}}$ declines by $0.1\,\mathrm{Wm}^{-2}$ per $0.5\,\mathrm{PW}$ increase (see dotted, red graph in figure 15). We observe an abrupt change in the tendency for $\mathrm{OHT}_{\mathrm{max}} = 2.5\,\mathrm{PW}$ at which pronounced tropical and subtropical atmospheric cooling sets in. This indicates that the change in the temperature difference between equatorial and tropical regions cause a drastic change in the dynamical properties of the system.

The reason for this enhanced decrease in $\overline{\dot{W}}$ can be found in the decrease of the temperature difference between ~~the~~ warm and ~~the~~ cold reservoir. From energy conservation we know~~,~~ the decrease in ~~the~~ strength of Lorenz energy cycle $\overline{\dot{W}}$ implies that ~~also~~ the total dissipation $\overline{\dot{D}}$ decreases in a steady state climate, as the climatic engine has smaller rate of transformation of available into kinetic energy. The decrease of $\overline{\dot{D}}$ implies, e.g. that surface winds are weaker, because this is where most of the dissipation takes place. We note that by increasing $\mathrm{OHT}_{\mathrm{max}}$, warm and cold air masses get mixed more effectively with the result that the atmosphere becomes horizontally more isothermal and, hence, the climatic engine acts less ~~efficient~~.

A closer look into the global energetics is provided by the reservoirs, conversions and sources following the classical Lorenz energy cycle where the atmospheric flow has been partitioned into the zonal mean and the eddy component (Fig. 16). ~~In accordance to~~ the change in $\Delta\Theta$ the available potential energies of the mean flow (P_{M}) and of the eddies (P_{E}) decrease. However, while the relative decrease in P_{M} and P_{E} is of the same size, the absolute values of P_{M} are substantially larger. A closer examination reveals a fundamental difference between the sensitivity of $\Delta\Theta$ and the total Lorenz–reservoir ($P_{\mathrm{M}} + P_{\mathrm{E}}$). While the decrease of $\Delta\Theta$ slows down for $\mathrm{OHT}_{\mathrm{max}} \leq 2.5$, the Lorenz–reservoir shows an almost linear decrease for the whole range of OHT changes. Only for P_{E} less sensitivity for larger OHT can be found.

Compared to the $\mathrm{OHT}_{\mathrm{max}} = 0\,\mathrm{PW}$ simulation, P_{M} is reduced by about 71 % in the $\mathrm{OHT}_{\mathrm{max}} = 4\,\mathrm{PW}$ run. The relative decrease for P_{E} and K_{M} is approx. 69 and 65 %, respectively. K_{E} declines by about 54 %.

Though diagnosed as residuals from the conversions, the total source of available potential energy and the total sink of kinetic energy are in good agreement with $\overline{\dot{W}}$ and η indicating a change in sensitivity at $\mathrm{OHT}_{\mathrm{max}} = 2.5\,\mathrm{PW}$. We notice that only the zonally symmetric heating generates avail-

able potential energy while the zonally asymmetric heating extracts P_{E}, i.e. it acts to homogenize the zonal temperature profiles. For the dissipation of kinetic energy, the eddy component is larger than the contribution of the zonal mean flow. For increasing OHT the magnitude of all sources/sinks decrease and both the (negative) eddy source of available potential energy and the zonal mean sink of kinetic energy go to zero.

In addition we note that assigning the overall strength of the Lorenz energy cycle to the zonal mean and the eddy flow would lead to different results depending whether we choose the generation of available potential energy $\overline{\dot{W}}$ or the dissipation of kinetic energy $\overline{\dot{D}}$ as measure. Dominant processes of the generation of available energy (i.e. $\overline{\dot{W}}$) are related to the zonal mean circulation while the dissipation of kinetic energy ($\overline{\dot{D}}$) acts on the eddies resulting from baroclinic instability. In addition, one may use the conversion ~~form~~ potential to kinetic energy to define the energy cycles strength. Here the baroclinic eddies accomplish the transformation while the zonal mean flow generates P_{M} on the expense of K_{M}, i.e. by favoring a thermal indirect circulation.

The overall decline in the reservoirs and sources with increasing OHT is also present for conversion terms which are related to the baroclinic conversion, i.e. $C(P_{\mathrm{M}}, P_{\mathrm{E}})$, $C(P_{\mathrm{E}}, K_{\mathrm{E}})$ and $C(K_{\mathrm{E}}, K_{\mathrm{M}})$. The conversion $C(P_{\mathrm{M}}, K_{\mathrm{M}})$ which is related to the zonal mean circulation show little changes.

Overall, the sensitivity of the eddy related conversions appears to decrease following the temporal sequence of a baroclinic life cycle: The conversion from zonal mean available potential energy to eddy potential energy $C(P_{\mathrm{M}}, P_{\mathrm{E}})$ shows the largest sensitivity (approx. 65 %). The sensitivity of the transformation into eddy kinetic energy $C(P_{\mathrm{E}}, K_{\mathrm{E}})$ amounts to approx. 57 %, and the change of the conversion into zonal mean kinetic energy $C(K_{\mathrm{E}}, K_{\mathrm{M}})$ is the smallest (approx. 53 %). However, to verify whether these changes are due to changes in the baroclinic life cycles or just a coincidence, further analysis is necessary, which is beyond the scope of the present paper.

Material entropy production $\overline{\dot{S}_{mat}}$ and the degree of irreversibility α are shown in figure 17 (left). As introduced in Appendix B, $\overline{\dot{S}_{mat}}$ is given by the sum of the minimum value of entropy production ($\overline{\dot{S}_{min}}$) compatible with the presence of the average dissipation and the excess of entropy production ($\overline{\dot{S}_{exc}}$) with respect to such minimum, i.e.

$$\overline{\dot{S}_{mat}} = \overline{\dot{S}_{min}} + \overline{\dot{S}_{exc}}$$

The ratio between $\overline{\dot{S}_{exc}}$ and $\overline{\dot{S}_{min}}$ defines the degree of irreversibility α,

$$\alpha = \frac{\overline{\dot{S}_{exc}}}{\overline{\dot{S}_{min}}}$$

and determines the ratio between the contributions to entropy production by down–gradient turbulent transport and by viscous dissipation of mechanical energy.

With increasing values of $\mathrm{OHT_{max}}$, the decrease in the intensity of the Lorenz energy cycle and the increase in the surface temperature imply a reduction of the part in $\overline{\dot{S}_{mat}}$ linked with frictional dissipation, which is related to lower bound of entropy production $\overline{\dot{S}_{min}}$. Nonetheless, one needs to investigate the excess of entropy production $\overline{\dot{S}_{exc}}$, which is linked to the turbulent heat fluxes down the temperature gradient. The relative decrease in entropy production due to frictional dissipation ($\overline{\dot{S}_{min}}$) is stronger than the relative decrease in entropy production by down–gradient turbulent heat transport ($\overline{\dot{S}_{exc}}$) as featured by the overall increase in α (figure 17). Thus, the entropy production due to the turbulent heat transport down the gradient of the temperature field becomes more and more dominant as the oceanic transport increases because irreversible mixing becomes stronger.

In figure 17 (right) the main contributions of the material entropy production in the model are displayed. This includes the contributive processes due to latent and sensible turbulent heat fluxes and frictional dissipation of kinetic energy. Entropy production due to latent heat processes, including convective as well as large–scale precipitation, surface latent heat fluxes and rain–snow conversion processes, makes by far the largest portion of material entropy production. For small $\mathrm{OHT_{max}}$, the value of entropy production by latent heat reads $35\,\mathrm{mW\,m^{-2}\,K^{-1}}$. For increasing $\mathrm{OHT_{max}}$ up to $1.5\,\mathrm{PW}$ the value increases by $2\,\mathrm{mW\,m^{-2}\,K^{-1}}$, while for larger $\mathrm{OHT_{max}}$, this contribution to entropy production declines by $4\,\mathrm{mW\,m^{-2}\,K^{-1}}$. Entropy production by frictional dissipation decreases from $8\,\mathrm{mW\,m^{-2}\,K^{-1}}$ for $\mathrm{OHT_{max}} = 0\,\mathrm{PW}$ to $3\,\mathrm{mW\,m^{-2}\,K^{-1}}$ for $\mathrm{OHT_{max}} = 4\,\mathrm{PW}$. Entropy production by sensible turbulent heat flux at the surface as well as in the atmosphere decreases by half (from $2\,\mathrm{mW\,m^{-2}\,K^{-1}}$ to $1\,\mathrm{mW\,m^{-2}\,K^{-1}}$) with $\mathrm{OHT_{max}}$ increasing. One would expect that larger values of $\mathrm{OHT_{max}}$ would lead to larger values of $\overline{\dot{S}_{mat}}$, using the argument that a warmer planet should be able to have a stronger hydrological cycle. For low values of $\mathrm{OHT_{max}}$, the increase in $\overline{\dot{S}_{mat}}$ due to the hydrological cycle is overcompensated by the decrease in the contribution due to the frictional dissipation.

In order to further clarify the impacts on the material entropy production of increasing $\mathrm{OHT_{max}}$, we split the material entropy production due to irreversible latent turbulent heat processes ($\boldsymbol{F}_{lat}$ in eq. B6) into the contributions coming from individual parameterizations (processes) operating in our model which are convective precipitation, large–scale precipitation, surface latent heat fluxes, and the heat release due to rain–snow conversion. Figure 18 displays the time mean of these contribution coming from each latitudinal belt. Positive contributions indicate a warming while negative contributions are related to a cooling due to the respective process.

Convective precipitation gives the largest positive contribution, particularly in the tropics and subtropics. For increased $\mathrm{OHT_{max}}$ we observe that the peak at the equator is significantly reduced while convection processes move into the mid–latitudes where the surface is heated and static stability decreases. The positive contribution from large-scale precipitation features are shifted out of the mid–latitudes towards higher latitudes with increasing $\mathrm{OHT_{max}}$. As large-scale precipitation regimes experience a shift to higher latitudes, their maximum intensity is almost kept constant. The contri-

bution by the surface latent heat flux is negative related to surface cooling. For 0 PW, the magnitude has its ~~s~~ maximum at latitudes of $20°$ to $25°$ indicating the region with maximum evaporation. As the heat transport in the ocean is increased, latent turbulent heat fluxes reduces largely in tropical and subtropical regions, and peak latent heat fluxes move towards mid–latitudes. The region with largest evaporation at the surface shifts from the subtropics to the mid-latitudes with increasing $\mathrm{OHT}_{\mathrm{max}}$. The contribution from latent heat release by rain-snow conversion is negative (indicating an overall cooling) and qualitatively shows similar patterns as the meridional profile for convective processes.

Figure18 seems to imply that the tropical latitudinal belt features a negative material entropy production. This is indeed not the case, because there is a net large scale transport of energy from those regions to both the equator and the mid–latitudes as a result of a net moisture export (figure 5). Such a negative contribution is overcompensated by the positive material entropy production associate to the absorption of the transported latent heat taking place elsewhere.

5 Summary and discussion

We have studied the impact of the oceanic heat transport (OHT) on the atmospheric circulation focusing on two important aspects: changes in the atmospheric meridional heat transport, and changes in global thermodynamic properties of the atmosphere including efficiency, irreversibility and the Lorenz energy cycle.

Using a general circulation model of intermediate complexity (PlaSim) including an oceanic mixed–layer we have adopted an experimental design from Rose and Ferreira (2013). Here, an imposed oceanic heat transport of simple analytic form and with varying strength allows for systematic analyses.

We found a compensation of the changes in oceanic heat transport by the atmosphere ~~in consistence~~, with Stone's (1978) conclusions. The presence of sea–ice may explain the deviations from a perfect compensation as discussed in Enderton and Marshall (2008). While all components of the atmospheric heat transport are affected by the compensation, their relative importance for the total transport remains almost unchanged. While the atmosphere compensates very effectively the changes in the OHT, so that the total meridional heat transport is weakly altered, the climate as a whole strongly depends on the chosen value of the OHT. The basic reason for this is that the atmosphere and the ocean transport heat at different heights and across different temperature gradients.

In agreement with Rose and Ferreira, we have found an increase of the global mean near–surface temperature and a decrease of the equator–to–pole temperature gradient with increasing OHT for $\mathrm{OHT}_{\mathrm{max}} < 3$ PW. For larger OHT, the temperature gradient still decreases but the global average remains constant. For the tropics, there is a significant decrease of both temperature and its gradient for $\mathrm{OHT}_{\mathrm{max}} > 2$ PW, with a reversal of the gradient for $\mathrm{OHT}_{\mathrm{max}} > 3$ PW. For smaller OHT, we observed a slight warming and a reduction of the gradient with increasing OHT. The latter is consistent with

results from Koll and Abbot (2013). However, in their aqua-planet the tropical temperature show little sensitivity with small increases for all imposed (positive) OHTs (up to 3 PW).

A tropical cooling for imposed oceanic heat transports somewhat larger than present-day values has also been found by Barreiro et al. (2011) in a more complex coupled atmosphere-slab ocean model with present–day land–sea distribution. They argue that this suggests present–day climate being close to a state where the warming effect of OHT is maximized. Barreiro et al. related the tropical cooling to a strong cloud–SST feedback and showed that the results are sensitive to the particular parameterizations. Though our simulations are highly idealized and do not represent all the complexities of the real climate system, it is interesting to note that we find almost no further increase of the global near surface temperature for $\mathrm{OHT}_{\mathrm{max}} > 2.5\,\mathrm{PW}$ and maxima in Θ^+ and Θ^- at about the same value of OHT.

Confirming the results of previous studies (Herweijer et al., 2005; Barreiro et al., 2011; Koll and Abbot, 2013) we have found a decrease of the Hadley cell for increasing OHT. In addition, the Hadley cell broadens and the maxima of the Hedley and the Ferrel cell shift polward when OHT obtains large values ($\mathrm{OHT}_{\mathrm{max}} > 2.5\,\mathrm{PW}$).

Sea–ice gradually decreases with increasing OHT. Though on annual average sea–ice is present for all simulations, for $\mathrm{OHT}_{\mathrm{max}} > 2\,\mathrm{PW}$ areas of open water are present for all latitudes during summer. This may suggest that sea–ice is playing an important role in controlling the global mean temperature and/or the position of the Ferrel cell. However, we did not find sufficient evidence to support this hypothesis.

Separating individual sources by applying the Kuo–Eliassen equation showed that the characteristics of the Hadley cell can be explained by the mean meridional circulations related to the diabatic heating and, to a smaller extent, to the friction. In our simulations, the meridional circulation induced by friction also controls the behavior of the Ferrel cell. Eddy transports of heat and momentum appear to be less important. This is different from results by Kim and Lee (2001b) where the mean meridional circulation related to eddy fluxes account for about 50 % of the Ferrel cell's strength. The coarse vertical resolution may be responsible for a reduced eddy activity.

In agreement with Czaja and Marshall (2006) the total atmospheric meridional heat transport is related to the strength of the transformed Eulerian mean residual mean streamfunction and the contrast of moist static energy across the circulation. As obtained by scale analysis by Czaja and Marshall, the residual mean streamfunction in the mid–latitudes is dominated by the so called eddy stress which is given by the meridional transport of (moist) static energy.

The response of global thermodynamical properties of the climate system has been studied following a theoretical framework introduced by Lucarini (2009).

Increasing OHT leads to the reduction in the difference between the warm pool temperature Θ^+ and the cold pool temperature Θ^-. The latter implies that the atmospheric system becomes more isothermal in the horizontal. The temperature difference between the warm (Θ^+) and the cold (Θ^-)

heat reservoir decreases for increasing oceanic heat transport. This is basically caused by enhanced warming in the extratropics and by tropical cooling for increasing OHT. Main driver for this is the poleward relocation of latent heat release patterns (not shown). This may lead to further warming due to the water vapour feedback (Herweijer et al., 2005; Barreiro et al., 2011).

The effect of thermalisation leading to the reduction of the efficiency of the system with increasing intensity of the ocean heat transport can be related to the decrease in the reservoir of the potential energy available for conversion in the Lorenz energy cycle. The strength of the Lorenz energy cycle linearly decreases with increasing OHT. A change to smaller sensitivity is observed at $\mathrm{OHT}_{\mathrm{max}} = 2.5\,\mathrm{PW}$.

The magnitude of all reservoirs and conversions of the Lorenz energy cycle decreases with increasing OHT. However, the sensitivities differ. P_{M} and the conversion from P_{M} to P_{E} exhibit the largest changes. Eddy kinetic energy, the barotropic conversion from eddy kinetic energy to zonal mean kinetic energy, and the conversion from zonal mean kinetic energy to P_{M} are least affected

When considering stronger oceanic transport, the climate system is characterized by a declining total material entropy production, while the degree of irreversibility increases, since the decrease in entropy production by frictional dissipation is more intense than the decrease in entropy generation due to sensible and, in particular, latent heat flux. The flux of latent heat contributes most to the material entropy production in the climate system. When increasing the heat transport in the ocean from $0.0\,\mathrm{PW}$ to $1.5\,\mathrm{PW}$, material entropy production due to latent heat flux increases which can be explained by an outspread of convection from the deep tropics into the mid latitudes, while the maximum latent release is still located in the central tropics. When increasing the heat transport further, convective processes collapse in the deeps tropics and, thus, affecting evaporation intensities at tropical sea surface by reducing it. As a result, a decrease in material entropy production by latent heat fluxes can be noted from the increase of the oceanic heat transport larger than $2.0\,\mathrm{PW}$.

Overall, our study demonstrates the large impact of the oceanic heat transport on the atmospheric circulation effecting the zonally symmetric flow, the zonally asymmetric flow and the interaction between both. By reducing the meridional temperature gradient, an increased oceanic heat transport slows down the atmospheric mean meridional circulation and shifts the Hadley and the Ferrel cell. In addition changes in OHT substantially modify global thermodynamic properties like the strength of the Lorenz energy cycle, the efficiency, the entropy production and the irreversibility.

The reduction of the meridional gradient of the surface temperature is one of the major features of global warming. Lu et al. (2007) showed a consistent weakening and poleward expansion of the Hadley cell in IPCC AR4 simulations. Hence, changes in the oceanic heat transport may significantly modify the response of the atmospheric circulation to greenhouse warming. A weakening of the oceanic meridional overturning circulation, as predicted by the majority of coupled ocean–atmosphere general circulation models (though with large uncertainties; IPCC, 2013), would therefore act as a negative feedback mechanism. This negative feedback might become even more im-

portant when strong melting of inland ice sheets, due to global warming, is taken into account. The associated input of large amounts of fresh water has a huge potential to slow down the oceanic circulation.

Complementing the investigation by Rose and Ferreira (2013) and helping to understand the properties of warm equable climates a subsequent study may focus on the role of latitudinal location of the peak OHT. In the present set of experiments the peak oceanic transport was fixed at the latitude of 27°. Due to the local atmospheric compensation, this preferentially affects the atmospheric heat transport components relevant in this region which is the eddy transport of latent heat. The overall response may be different if the OHT peak is located in regions where other components of the atmospheric heat transport are more important.

Another possible future line of investigation may deal with studying planets with different astrophysical parameters, such as rotation rate, eccentricity, and obliquity, with the goal of contributing to the rapidly growing field of investigation of the atmospheres of exoplanets.

Appendix A: The mean meridional circulation

To analyse the mean meridional circulation we make use of the so called Kuo–Eliassen equation (Kuo, 1956; Eliassen, 1951). It is a diagnostic equation which relates the mean meridional circulation (i.e. Hadley, Ferrel and Polar cell) to different sources.

Applying the quasi-geostrophic approximation and defining a streamfunction ψ with

$$[v] = \frac{g}{2\pi r \cos\phi}\frac{\partial \psi}{\partial p}$$

$$[\omega] = -\frac{g}{2\pi r \cos\phi}\frac{\partial \psi}{r\partial \phi}$$

the Kuo–Eliassen equation may be derived as (see, e.g., Peixoto and Oort, 1992, Chap. 14.5.5)

$$\begin{aligned}\frac{f^2 g}{2\pi r\cos\phi}\frac{\partial^2\psi}{\partial p^2} - \frac{g}{2\pi r^3 \rho[\theta]}\frac{\partial}{\partial\phi}\left(\frac{\partial[\theta]}{\partial p}\frac{\partial\psi}{\partial\phi}\right) = &\frac{1}{r\rho[T]}\frac{\partial}{\partial\phi}\frac{[Q]}{c_p}\\ &- f\frac{\partial[F]}{\partial p}\\ &- \frac{1}{r^2\rho[\theta]}\frac{\partial}{\partial\phi}\frac{\partial[v^*\theta^*]\cos\phi}{\cos\phi\partial\phi}\\ &+ \frac{f}{r\cos^2\phi}\frac{\partial^2[u^*v^*]\cos^2\phi}{\partial p\partial\phi}\end{aligned}$$

where, in addition to the symbols defined above, f is the Coriolis parameter, ρ density, θ potential temperature, Q diabatic heating and F the tendency of the zonal wind due to friction.

We solve the Kuo–Eliassen equation for ψ by applying an iterative method (Gauss–Seidel method) to its finite difference approximation. Thus, we are able to diagnose the contributions from the different sources to the mean meridional circulation, which are diabatic heating (1st term r.h.s), friction (2nd), meridional eddy heat transport (3rd) and eddy momentum transport (4th). We note that, though

the equation, in the present form, involves the quasi-geostrophic approximation, it has shown to be reasonably applicable even in the deep tropics (Kim and Lee, 2001a, b). In addition, as pointed out by Kim and Lee, it should be noted that this diagnostics will only yield direct effect of the particular source. Since all processes are strongly interlinked changes in one source will lead to changes in other terms. For example, according to the equations of motion changes of the meridional eddy momentum transport will have consequences for the frictional dissipation of zonal mean momentum. These indirect effects cannot be identified with our (linear) methodology.

While the Kuo–Eliassen equation gives us the classical three cell picture of the mean meridional circulation the transformed Eulerian mean (TEM) formalism (Andrews and McIntyre 1976) provides a closer link to the total atmospheric meridional heat transport.

Defining the residual streamfunction ψ_{res} with

$$v_{res} = \frac{g}{2\pi r \cos\phi}\frac{\partial \psi_{res}}{\partial p}$$

$$\omega_{res} = -\frac{g}{2\pi r \cos\phi}\frac{\partial \psi_{res}}{r\partial \phi}$$

and

$$v_{res} = [v] - \frac{\partial}{\partial p}\left(\frac{[v^*\theta^*]}{\partial \theta_s/\partial p}\right)$$

$$\omega_{res} = [\omega] + \frac{1}{r\cos\phi}\frac{\partial}{\partial \phi}\left(\frac{[v^*\theta^*]\cos\phi}{\partial \theta_s/\partial p}\right)$$

an equation similar to the Kuo–Eliassen equation can be obtained for ψ_{res}

$$\frac{f^2 g}{2\pi r\cos\phi}\frac{\partial^2\psi_{res}}{\partial p^2} - \frac{g}{2\pi r^3\rho[\theta]}\frac{\partial}{\partial\phi}\left(\frac{\partial\theta_s}{\partial p}\frac{\partial\psi_{res}}{\partial\phi}\right) = \frac{1}{r\rho[T]}\frac{\partial}{\partial\phi}\frac{[Q]}{c_p} - f\frac{\partial[F]}{\partial p} - \frac{f}{r\cos\phi}\frac{\partial(div\boldsymbol{F})}{\partial p}$$

Here the total effect of the eddies on the meridional circulation (viewed from a Lagrangian perspective) is given by the divergence of the Eliassen–Palm flux with

$$F_\phi = -r\cos[u^*v^*]$$

$$F_p = f\,r\cos\phi\frac{[v^*\theta^*]}{\partial\theta_s/\partial p}$$

Cazja and Marshall (2006) showed that the atmospheric heat transport can be represented by the product of the strength of the TEM residual circulation and the vertical contrast in moist static energy (or equivalent potential tempertaure θ_e) if the eddy transport of ~~*theta*~~ is replaced by the transport of ~~*theta*~~.

Appendix B: Non–equilibrium thermodynamics

Let Ω be the volume domain of the climate system and $\dot{Q}$ be the local heating rate due to frictional dissipation and convergence of heat fluxes including radiative, sensible and latent heat components. At each instant t we divide Ω into two subsections, so that $Q(x,t) > 0, x \in \Omega^+$ defining Q^+, and $Q(x,t) < 0, x \in \Omega^-$ for Q^- respectively. We wish to remark that the domains Ω^+ and Ω^- are time dependent. Integrating the two heating components results in: $\int_{\Omega^+} \rho \dot{Q}^+ \mathrm{d}V + \int_{\Omega^-} \rho \dot{Q}^- \mathrm{d}V = \dot{\Phi}^+ + \dot{\Phi}^-$. Johnson (2000) and Lucarini (2009) show that the time average $\overline{\dot{\Phi}^+} + \overline{\dot{\Phi}^-}$ gives the rate of generation of available potential energy, so that:

$$\overline{\dot{W}} = \overline{\dot{\Phi}^+} + \overline{\dot{\Phi}^-}. \tag{B1}$$

The efficiency of the climate machine can now be expressed as:

$$\eta = \frac{\overline{\dot{\Phi}^+} + \overline{\dot{\Phi}^-}}{\overline{\dot{\Phi}^+}}. \tag{B2}$$

This expression represents the ratio for the work output $\overline{\dot{\Phi}^+} + \overline{\dot{\Phi}^-}$ to the heat input $\overline{\dot{\Phi}^+}$. At each instant one defines the quantities $\Sigma^{+(-)} = \frac{\int_\Omega^{+(-)} \rho \dot{Q}^{+(-)}}{T}$, which are the instantaneous entropy sources and sinks in the system. As explained in Johnson (2000) and Lucarini (2009), we have that $\overline{\dot{\Sigma}^+} + \overline{\dot{\Sigma}^-} = 0$. We can then introduce the scale temperatures $\Theta^+ = \frac{\overline{\dot{\Phi}^+}}{\overline{\dot{\Sigma}^+}}$ and $\Theta^- = \frac{\overline{\dot{\Phi}^-}}{\overline{\dot{\Sigma}^-}}$, so that eq. B2 can be rewritten as

$$\eta = \frac{\Theta^+ - \Theta^-}{\Theta^+} \tag{B3}$$

where $\Theta^+ > \Theta^-$.

Hence, the motion of the general circulation of the system can be sustained against friction because zones being already relatively warm absorb heat whereas the relatively low temperature zones are cooled.

The Lorenz energy cycle can thus be seen as resulting from the work of an equivalent Carnot engine operating between the two (dynamically determined) reservoirs at temperature Θ^+ and Θ^-. Yet, the climate is far from being a perfect engine, as many irreversible processes take place; nonetheless, a Carnot–equivalent picture can be drawn as described.

Let us now delve into such irreversible processes. In the climate system two rather different sets of processes contribute to the total entropy production (Peixoto and Oort, 1992; Goody, 2000; Ambaum, 2010). The first set of processes is responsible for the irreversible thermalisation of photons emitted near the Sun's corona at roughly 5800 K, absorbed and then re–emitted at much lower temperatures, typical of the Earth's climate ($\sim$255 K). This gives the largest contribution

to the total average rate of entropy production for the Earth system of about $900\,\mathrm{mW\,m^{-2}\,K^{-1}}$ (Peixoto and Oort, 1992; Ambaum, 2010). The remaining contribution is due to the processes responsible for mixing and diffusion inside the fluid component of the Earth system, and for the dissipation of kinetic energy due to viscous processes. This constitutes the so–called material entropy production, and is considered to be the entropy related quantity of main interest as far as the properties of the climate system are concerned. Further relevant research on entropy production in the climate system treating also the geochemical and radiative contribution to entropy production can be found in Kleidon (2009) and Wu and Liu (2010) respectively.

The entropy budget of geophysical fluids at steady state, following Goody (2000); Lucarini et al. (2011), is given by:

$$\overline{\dot{S}(\Omega)} = \int_{\Omega} \rho \left(\overline{\frac{\dot{q}_{rad}}{T}} + \overline{\dot{s}_{mat}} \right) \mathrm{d}V = 0, \tag{B4}$$

where $\dot{q}_{rad}$ indicates the heating rate by the convergence of radiative fluxes, T is the local temperature at which the energy is gained or lost, while $\dot{s}_{mat}$ represents the density of entropy production associated with the irreversibility of processes involving the fluid medium. Eq. B4 represents the entropy budget and states that in a steady state the radiative entropy source must be balanced by the rate of material entropy production $\dot{S}_{mat}$ due to material irreversible processes. See a detailed discussion of this aspect in Lucarini and Pascale (2014), where the contributions to the material entropy production at various spatial and temporal scales are discussed.

In a steady–state climate the material entropy production $\dot{S}_{mat}(\Omega)$ can be expressed in general terms as:

$$\overline{\dot{S}_{\mathrm{mat}}(\Omega)} = \int_{\Omega} \rho \overline{\dot{s}_{mat}} \mathrm{d}V = \int_{\Omega} \overline{\frac{\varepsilon^2}{T}} \mathrm{d}V + \int_{\Omega} \overline{(\boldsymbol{F}_{sens} + \boldsymbol{F}_{lat}) \cdot \boldsymbol{\nabla} \frac{1}{T}} \mathrm{d}V = - \int_{\Omega} \rho \overline{\frac{\dot{q}_{rad}}{T}} \mathrm{d}V, \tag{B5}$$

where $\overline{\dot{s}_{mat}}$ is the time averaged density of entropy production due to the following irreversible processes inside the medium: dissipation of kinetic energy (ε^2 is the specific dissipation rate) and turbulent transport of heat down the temperature gradient ($\boldsymbol{F}_{sens}$ and $\boldsymbol{F}_{lat}$, being the sensible and latent turbulent heat fluxes, respectively).

One needs to underline that a more refined treatment of the entropy production related to the hydrological cycle has been proposed by e.g. Pauluis and Held (2002a), Pauluis and Held (2002b) and Romps (2008). Nonetheless, as discussed in Lucarini et al. (2014), the overall contribution of the entropy production due to the hydrological cycle can be reconstructed to a high degree of accuracy also in the simplified method proposed here.

Note that one can compute the entropy production as:

$$\overline{\dot{S}_{\mathrm{mat}}(\Omega)} = \int_{\Omega} \overline{\frac{\varepsilon^2}{T}} \mathrm{d}V + \int_{\Omega} \overline{\frac{-\boldsymbol{\nabla} \cdot (\boldsymbol{F}_{sens} + \boldsymbol{F}_{lat})}{T}} \mathrm{d}V + \int_{\partial\Omega} \overline{\frac{\boldsymbol{F}_{sens} + \boldsymbol{F}_{lat}}{T}} \cdot \hat{n} \mathrm{d}S, \tag{B6}$$

where the first term is unchanged, the second terms describes the entropy gain and loss due to heating and cooling by convergence of sensible and latent turbulent heat fluxes, and the last term is the net entropy flux across the boundaries of Ω. If one consider the atmospheric domain as Ω, such term becomes equal to the integral at surface of the ratio between the sum of the sensible and of the latent heat flux divided by the surface temperature. Eq. B6 represents the way entropy production is typically computed in numerical models. If one considers the whole climate system as Ω, the boundary terms disappear. Nonetheless, another term proportional to a Dirac's delta at $z = z_{surf} = 0$ appears, resulting from the divergence of the turbulent flux due to the net evaporation at surface. If we integrate over Ω, corresponding to the whole climate system, the contribution of this term is exactly the same as in the case where Ω corresponds to the atmosphere only. In other terms, our simplified, non–dynamical representation of the ocean is such that all the entropy is produced in the atmosphere.

We can now separate in eq. B5 - or, equivalently, in eq. B6 the first term from the rest, so that, following Lucarini (2009), the material entropy production can be expressed as:

$$\overline{\dot{S}_{mat}(\Omega)} = \overline{\dot{S}_{min}(\Omega)} + \overline{\dot{S}_{exc}(\Omega)}, \tag{B7}$$

where $\overline{\dot{S}_{min}(\Omega)}$ is the minimum value of entropy production compatible with the presence of average dissipation rate $\int_\Omega \epsilon^2 \mathrm{d}V$, while $\overline{\dot{S}_{exc}(\Omega)}$ is the excess of entropy production with respect to such minimum. One can associate $\overline{\dot{S}_{min}}$ exactly with the term in eq. B5 related to the dissipation of kinetic energy, while $\overline{\dot{S}_{exc}}$ can be identified with the sum of the other two terms.

If we take the ratio of the two terms on the right–hand side in eq. B7, we have that

$$\alpha = \frac{\overline{\dot{S}_{exc}(\Omega)}}{\overline{\dot{S}_{min}(\Omega)}} \approx \frac{\int_\Omega \overline{(\boldsymbol{F}_{sens} + \boldsymbol{F}_{lat}) \cdot \boldsymbol{\nabla} \frac{1}{T}} \mathrm{d}V}{\int_\Omega \overline{\frac{\varepsilon^2}{T}} \mathrm{d}V}, \tag{B8}$$

where α is the degree of irreversibility (Lucarini, 2009) and determines the ratio between the contributions to entropy production by down–gradient turbulent transport and by viscous dissipation of mechanical energy. If this ratio is close to zero ($\alpha \to 0$), all the production of entropy is exclusively caused by unavoidable viscous dissipation. If the turbulent heat transport in the system from high to low temperature regions is enhanced, then also entropy production increases. However, if the turbulent heat transport down the temperature gradient is maximised, the efficiency declines, since the temperature difference between the warm and cold reservoirs tends to become zero. The characterisation of the maximum entropy production principle (MEPP) suggests that the climate system adjusts in such a way to maximize the entropy production (Paltridge, 1975; Grassl, 1981; Kleidon and Lorenz, 2005).

Appendix C: The Lorenz energy cycle

The atmospheric energy cycle proposed by Lorenz (1955), is one of the most important concepts to understand the global atmospheric circulation by means of energy conservation and by considering the integrated effects of physical mechanisms involved, that is, e.g., the generation of available potential energy by external forcing, the dissipation of kinetic energy and the energy conversions by baroclinic and barotropic processes. At the same time it gives information about the relative importance of the zonal mean circulation, the eddies and the interaction between both.

Refering to the reservoirs of zonal available potential energy, eddy available potential energy, zonal kinetic energy and eddy kinetic energy as P_M, P_E, K_M and K_E, respectively, the Lorenz energy cycle (i.e. the budget equations) may be written as:

$$\frac{\mathrm{d}P_\mathrm{M}}{\mathrm{d}t} = [S_\mathrm{P}] - C(P_\mathrm{M}, P_\mathrm{E}) - C(P_\mathrm{M}, K_\mathrm{M})$$
$$\frac{\mathrm{d}P_\mathrm{E}}{\mathrm{d}t} = S^*_\mathrm{P} + C(P_\mathrm{M}, P_\mathrm{E}) - C(P_\mathrm{E}, K_\mathrm{E})$$
$$\frac{\mathrm{d}K_\mathrm{E}}{\mathrm{d}t} = S^*_\mathrm{K} + C(P_\mathrm{E}, K_\mathrm{E}) - C(K_\mathrm{E}, K_\mathrm{M})$$
$$\frac{\mathrm{d}K_\mathrm{M}}{\mathrm{d}t} = [S_\mathrm{K}] + C(K_\mathrm{E}, K_\mathrm{M}) + C(P_\mathrm{M}, K_\mathrm{M})$$

where $[S_\mathrm{P}]$, S^*_P, $[S_\mathrm{K}]$ and S^*_K are external sources/sinks of the respective quantities and $C(A, B)$ denotes the conversion from A to B.

To compute the individual contributions we follow the work of Ulbrich and Speth (1991). In pressure coordinates, the reservoirs are given by:

$$P_\mathrm{M} = \left\langle \frac{\gamma}{2}([T] - \{T\})^2 \right\rangle$$
$$P_\mathrm{E} = \left\langle \frac{\gamma}{2}[T^{*2}] \right\rangle$$
$$K_\mathrm{M} = \left\langle \frac{1}{2}([u]^2 + [v]^2) \right\rangle$$
$$K_\mathrm{E} = \left\langle \frac{1}{2}([u^{*2}] + [v^{*2}]) \right\rangle$$

and the conversion terms are:

$$C(P_\mathrm{M}, P_\mathrm{E}) = -\left\langle \gamma \left([v^*T^*] \frac{\partial [T]}{r \partial \phi} + [\omega^* T^*] \left(\frac{\partial ([T] - \{T\})}{\partial p} - \frac{R}{p \cdot c_p}([T] - \{T\}) \right) \right) \right\rangle$$
$$C(P_\mathrm{M}, K_\mathrm{M}) = -\left\langle \frac{R}{p}([\omega] - \{\omega\})([T_\mathrm{v}] - \{T_\mathrm{v}\}) \right\rangle$$
$$C(P_\mathrm{E}, K_\mathrm{E}) = -\left\langle \frac{R}{p}[\omega^* T^*_v] \right\rangle$$
$$C(K_\mathrm{M}, K_\mathrm{E}) = \left\langle \left([u^*v^*] \frac{\partial [u]}{r \partial \phi} + [u^*v^*][u] \frac{\tan\phi}{r} + [v^*v^*] \frac{\partial [v]}{r \partial \phi} \right.\right.$$
$$\left.\left. -[u^*u^*][v] \frac{\tan\phi}{r} + [\omega^*u^*] \frac{\partial [u]}{\partial p} + [\omega^*v^*] \frac{\partial [v]}{\partial p} \right) \right\rangle$$

with $[x]$ = zonal mean; x^* = deviation from zonal mean; $\{x\}$ = global horizontal mean; $\langle x \rangle = \frac{1}{g \cdot A} \int_A \int_p x \mathrm{d}p \mathrm{d}A$; A = horizontal Area; c_p = specific heat at const. pressure; g = gravity; p = pressure; r = radius of the Earth; R = gas constant; T = temperature; T_v = virtual temperature; u = zonal wind; v = meridional wind; ω = vertical (p) velocity; ϕ = latitude; γ = stability parameter $= -\frac{R}{p}\left(\frac{\partial[\overline{T}]}{\partial p} - \frac{R}{c_p}\frac{[\overline{T}]}{p}\right)^{-1}$.

The external sources/sinks are diagnosed from the respective residuals. We note that in Ulbrich and Speth these energetics were formulated for a mixed space–time domain. In our case, however, the contributions by stationary eddies are zero because of the zonally symmetric forcing.

We also note that by using above equations the computed annual averaged values include contributions from the annual cycle. It turns out, however, that only the reservoirs P_M and K_M, and the conversion $C(P_\mathrm{M}, K_\mathrm{M})$ are affected.

Acknowledgements. The authors wish to acknowledge support by the Cluster of Excellence CliSAP. V. Lucarini wishes to acknowledge the financial support provided by the ERC-Starting Investigator Grant NAMASTE – Thermodynamics of the Climate System (Grant no. 257106). We thank three anonymous reviewers for constructive criticism.

References

Ambaum, M. H. P. M.: Thermal physics of the atmosphere, volume 1, Wiley.com,2010.

Andrews, D. G., and McIntyre, M. E.: Planetary waves in horizontal and vertical shear: The generalized Eliassen–Palm relation and the mean zonal acceleration, J. Atmos. Sci., 33, 2031–2048, 1976.

Barreiro, M., Cherchi, A., and Masina, S.: Climate sensitivity to changes in ocean heat transport, J. Climate, 24, 5015–5030, 2011.

Boschi, R., Lucarini, V., and Pascale, S.: Bistability of the climate around the habitable zone: a thermodynamic investigation, Icarus, 226, 1724–1742, 2012.

Czaja, A. and Marshall, J.: The partitioning of poleward heat tansport between the atmosphere and ocean, J. Atmos. Sci., 63, 1498–1511, 2006

Eliassen, A.: Slow frictionally controlled meridional circulation in a circular vortex, Astro. Norv., 5, 19–60, 1951.

Enderton, D. and Marshall, J.: Explorations of atmosphere–ocean–ice climates on an aquaplanet and their meridional energy transports, J. Atmos. Sci., 66, 1593–1610, 2008.

Goody, R.: Sources and sinks of climate entropy. Q. J. Roy. Meteorol. Soc., 126,1953–1970, 2000.

Grassl, H.: The climate at maximum entropy production by meridional atmospheric and oceanic heat fluxes. Q. J. Roy. Meteorol. Soc., 107, 153–166, 1981.

Herweijer, C., Seager, R., Winton, M., and Clement, A.: Why ocean heat transport warms the global mean climate, Tellus A, 57, 662–675, 2005.

Hoskins, B. J., and Simmons, A. J.: A multi–layer spectral method and the semi–implicit method, Q. J. Roy. Meteorol. Soc., 101, 637–655, 1975.

IPCC: Climate Change 2013: The Physical Science Basis. Contribution of Working Group I to the Fifth Assessment Report of the Intergovernmental Panel on Climate Change, edited by: Stocker, T. F., Qin, D., Plattner, G.-K., Tignor, M., Allen, S. K., Boschung, J., Nauels, A., Xia, Y., Bex, V., and Midgley, P. M., Cambridge University Press, Cambridge, UK and New York, NY, USA, 1535 pp., 2013.

James, I. N. and Gray, L. J.: Concerning the effect of surface drag on the circulation of a planetary atmosphere, Q. J. Roy. Meteorol. Soc., 112, 1231–1250, 1986.

Johnson, D. R.: Entropy, the Lorenz energy cycle and climate. In General Circulation Model Development: Past, Present and Future, chapter 22, pages 659–720, Academic Press, 2000.

Kim, H.-K. and Lee, S.: Hadley cell dynamics in a primitive equation model. Part I: Axisymmetric flow, J. Atmos. Sci., 58, 2845–2858, 2001a.

Kim, H.-K. and Lee, S.: Hadley cell dynamics in a primitive equation model. Part II: Nonaxisymmetric flow, J. Atmos. Sci., 58, 2859–2871, 2001b.

Kleidon, A.: Nonequilibrium thermodynamics and maximum entropy production in the Earth system. Naturwissenschaften, 96, 653–677, 2009.

Kleidon, A. and Lorenz, R.: Entropy production by Earth system processes. In thermodynamics and the production of entropy. Springer DE. 2005.

Koll, D. D. B. and Abbot, D. S.: Why tropical sea surface temperature is insensitive to ocean heat transport changes, J. Climate, 26, 6742–6749, 2013.

Kuo, H.-L.: Forced and free meridional circulations in the atmosphere, J. Meteor., 13, 561–568, 1956.

Kuo, H.-L.: On formation and intensification of tropical cyclones through latent heat release by cumulus convection, J. Atmos. Sci., 22, 40–63, 1965.

Kuo, H.-L.: Further studies of the parameterization of the influence of cumulus convection on large–scale flow, J. Atmos. Sci., 31, 1232–1240, 1974.

Lacis, A. A. and Hansen, J. E.: A parameterization for the absorption of solar radiation on the Earth's atmosphere, J. Atmos. Sci., 31, 118–133, 1974.

Laursen, L. and Eliasen, E.: On the effects of the damping mechanisms in an atmospheric general circulation model, Tellus A, 41, 385–400, 1989.

Lorenz, E. N.: Available potential energy and the maintenance of the general circulation, Tellus, 7, 157–167, 1955.

Lorenz, E. N.: The nature and theory of the general circulation of the atmosphere. World Meteorological Organization, Geneva, 1967.

Louis, J. F.: A parametric model of vertical eddy fluxes in the atmosphere, Bound.-Lay. Meteorol., 17, 187–202, 1979.

Louis, J. F., Tiedtke, M., and Geleyn, M.: A short history of the PBL parameterisation at ECMWF, in: Proceedings, ECMWF Workshop on Planetary Boundary Layer Parameterization, Reading, 25–27 November 1981, 59–80, 1982.

Lu, J., Vecchi, G. A., and Reichler, T.: Expansion of the Hadley cell under global warming, Geophys. Res. Lett., 34, L06805, doi:10.1029/2006GL028443, 2007.

Lucarini, V.: Thermodynamic efficiency and entropy production in the climate system, Phys. Rev. E, 80, 021118, doi:10.1103/PhysRevE.80.021118, 2009.

Lucarini, V. and Pascale, : Entropy production and coarse graining of the climate fields in a general circulation model. Clim. Dyn., 43, 981–1000, 2014.

Lucarini, V. and Ragone, F.: Energetics of climate models: net energy balance and meridional enthalpy transport, Rev. Geophys., 49, RG1001, doi:10.1029/2009RG000323, 2011.

Lucarini, V., Fraedrich, K., and Lunkeit, F.: Thermodynamics of climate change: generalized sensitivities, Atmos. Chem. Phys., 10, 9729–9737, doi:10.5194/acp-10-9729-2010, 2010.

Lucarini, V., Fraedrich, K., and Ragone, F.: New results on the thermodynamical properties of the climate system. J. Atmos. Sci., 68. 2438–2458, 2011.

Lucarini, V., Pascale, S., Boschi, R., Kirk, E., and Iro, N.: Habitability and multistablility in earth–like plantets, Astron. Nachr., 334, 6, 576–588, 2013.

Lucarini, V., Blender, R., Pascale, S., Ragone, F., Wouters, J., and Herbert, C.: Mathematical and Physical Ideas for Climate Science, Rev. Geophys., 52, 809–859, 2014.

Paltridge, G.: Global dynamics and climate – a system of minimum entropy exchange. Q. J. Roy. Meteor. Soc., 101, 475–484, 1975.

Pauluis, O. and Held, I.: Entropy budget of an atmosphere in radiativeconvective equilibrium. Part I: Maximum work and frictional dissipation, J. Atmos. Sci., 59, 125–139, 2002a.

Pauluis, O. and Held, I.: Entropy budget of an atmosphere in radiativeconvective equilibrium. Part II: Latent heat transport and moist processes, J. Atmos. Sci., 59, 140–149, 2002b.

Peixoto, J. P. and Oort, A. H.: Physics of Climate, American Institute of Physics, New York, 1992.

Rind, D. and Chandler, M.: Increased ocean heat transports and warmer climate, J. Geophys. Res., 96, 7437–7461, 1991.

Roeckner, E., Arpe, K., Bengtsson, L., Brinkop, S., Dümenil, L., Esch, M., Kirk, E., Lunkeit, F., Ponater, M., Rockel, B., Sausen, R., Schlese, U., Schubert, S., and Windelband, M.: Simulation of the present–day climate with the ECHAM-3 model: impact of model physics and resolution, Meteorologie, Report No. 93, Max-Planck Institut für Meteorologie, Hamburg, 171 pp., 1992

Romanova, V., Lohmann, G., Grosfeld, K., and Butzin, M.: The relative roles of oceanic heat transport and orography on glacial climate, Quaternary Sci. Rev., 25, 832–845, 2006.

Romps, D. M.: The dry–entropy budget of a moist atmosphere. J. Atmos. Sci., 65, 3779–3799, 2008.

Rose, B. and Ferreira, D.: Ocean heat transport and water vapor greenhouse in a warm equable climate: a new look at the low gradient paradox, J. Climate, 26, 2117–2136, doi:10.1175/JCLI-D-11-00547.1, 2013.

Sasamori, T.: The radiatice cooling calculation for application to general circulation experiments, J. Appl. Meteorol., 7, 721–729, 1968.

Schröder, A., Lucarini, V., and Lunkeit, F.: The Impact of Oceanic Heat Transport on the Atmospheric Circulation: a Thermodynamic Perspective, Clim. Dynam., submitted, 2014.

Slingo, A. and Slingo, J. M.: Response of the National Center for Atmospheric Research community climate model to improvements in the representation of clouds, J. Geophys. Res., 96, 341–357, 1991.

Sloan, L. C., Walker, J. C. G., and Moore Jr., T. C.: Possible role of oceanic heat transport in early Eocene climate, Paleoceanography, 10, 347–356, 1995.

Stephens, G. L.: Radiation profiles in extended water clouds. II: Parameterization schemes, J. Atmos. Sci., 34, 2123–2132, 1978.

Stephens, G. L., Ackermann, S., and Smith, E. A.: A shortwave parameterization revised to improve cloud absorption, J. Atmos. Sci., 41, 687–690, 1984.

Stone, P. H.: Constraints on dynamical transports of energy on a spherical planet, Dynam. Atmos. Oceans, 2, 123–139, 1978.

Ulbrich, U. and Speth, P.: The global energy cycle of stationary and transient atmospheric waves: results from ECMWF analyses, Meteorol. Atmos. Phys., 45, 125–138, 1991.

Winton, M.: On the climate impact on ocean circulation, J. Climate, 16, 2875–2889, 2003.

Wu, W. and Liu, Y.: Radiation entropy flux and entropy production of the Earth system. Rev. Geophys., 48,1–27, 2010.

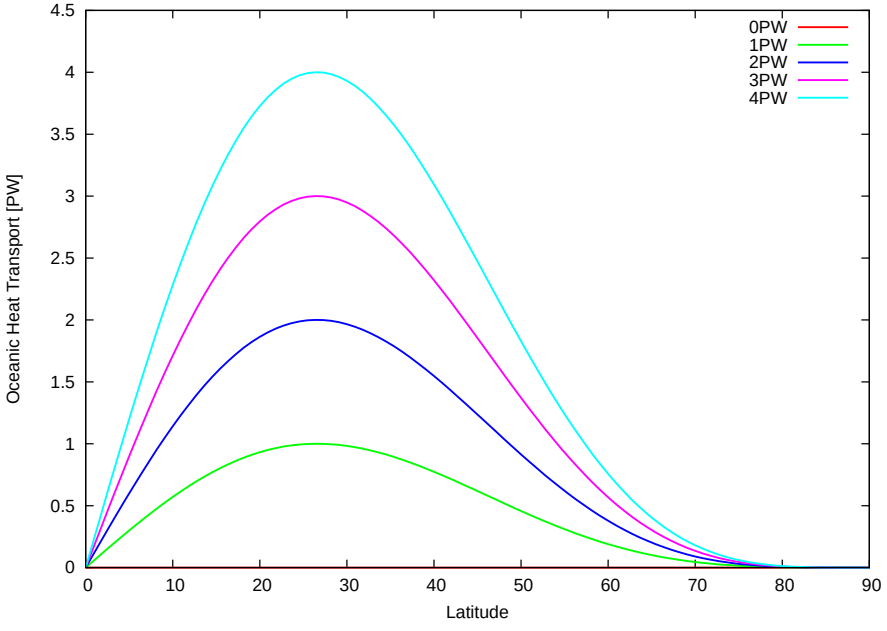

Figure 1. Oceanic heat transport (in PW) for $\mathrm{OHT}_{\mathrm{max}} = 0$, 1, 2, 3, and 4 PW.

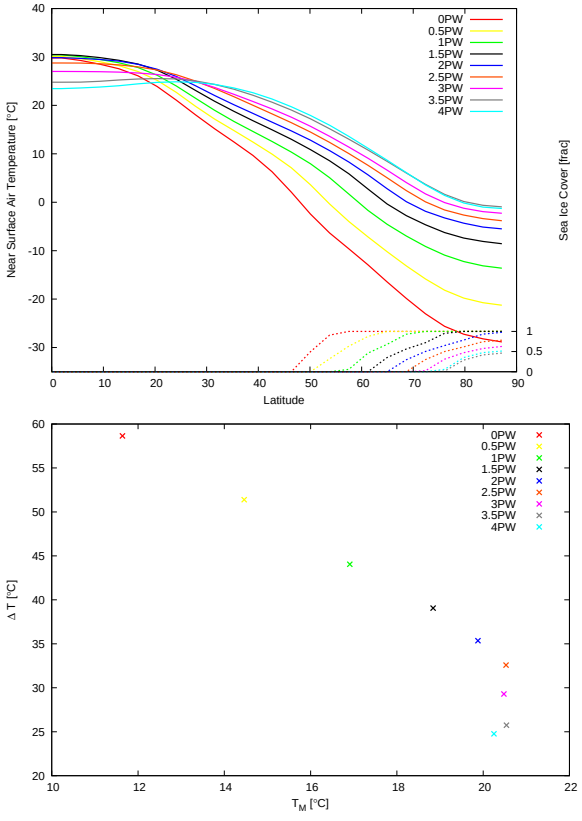

Figure 2. Climatological annual averages for all simulations: upper: zonal mean near-surface (solid lines) and sea–ice cover (dotted lines). temperature. Lower: global mean near–surface temperatures (T_{M}, in $^{\circ}$C) vs. equator-to-pol gradient (ΔT, in $^{\circ}$C).

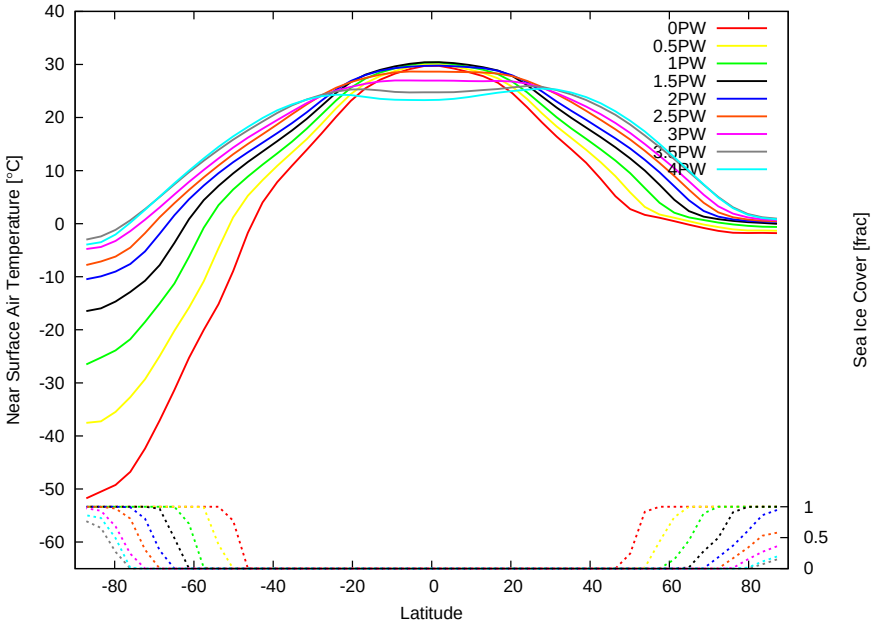

Figure 3. Climatological Northern Hemisphere summer (June–August) averages for all simulations: zonal mean near-surface temperatures (in °C; solid lines) and and sea–ice cover (dotted lines).

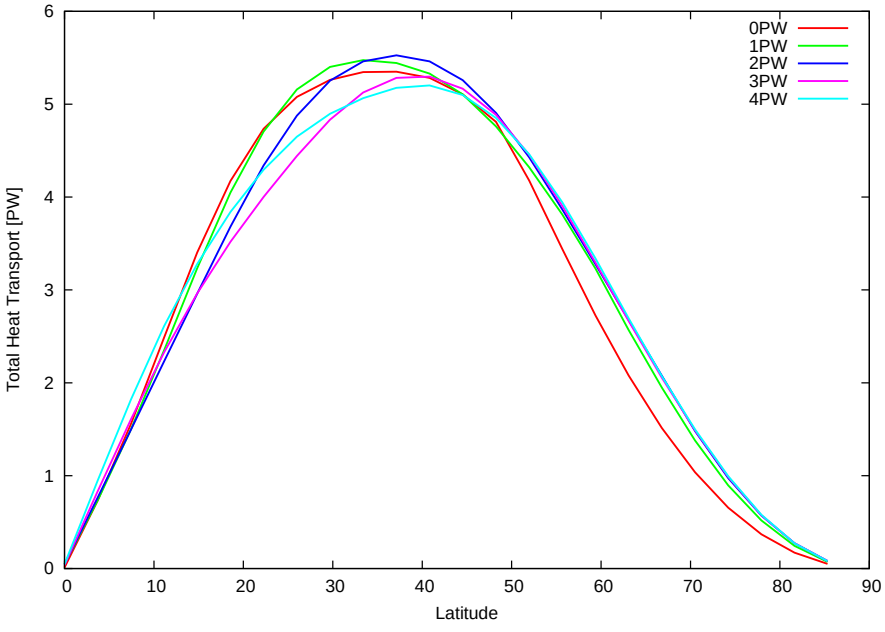

Figure 4. Total heat transport (in PW) diagnosed from energy budget at the top of the atmosphere for $\mathrm{OHT}_{\mathrm{max}} =$ 0, 1, 2, 3, and 4 PW.

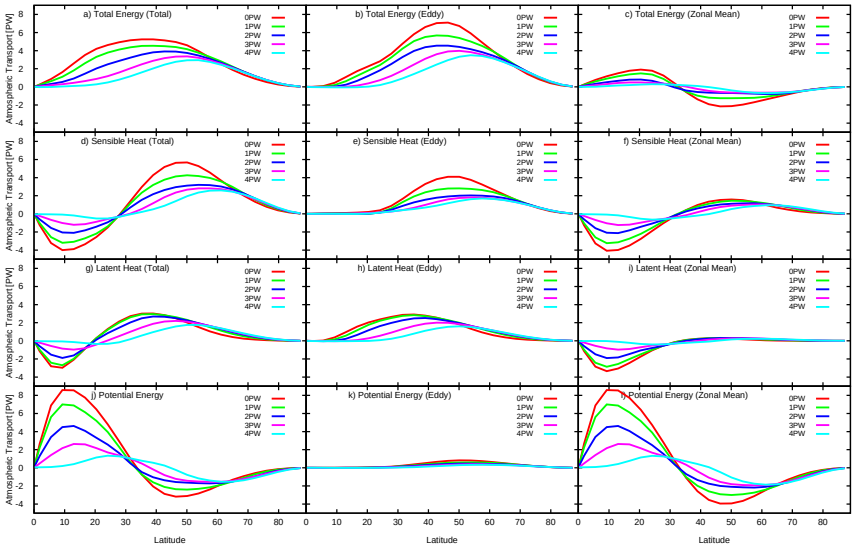

Figure 5. Atmospheric heat (moist static energy) transport (in PW) assigned to different processes for $\mathrm{OHT}_{\mathrm{max}} = 0$, 1, 2, 3, and 4 PW.

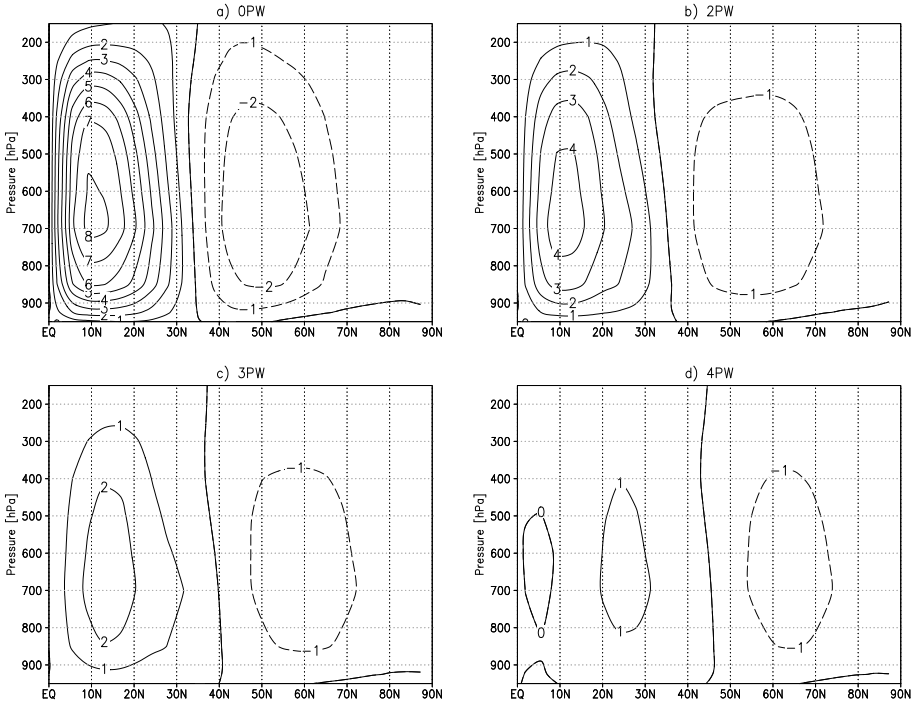

Figure 6. Climatological annual mean mass stream function (in $10^{10}\,\mathrm{kg\,s^{-1}}$) for $\mathrm{OHT}_{\mathrm{max}} = 0$, 1, 2, 3, and 4 PW.

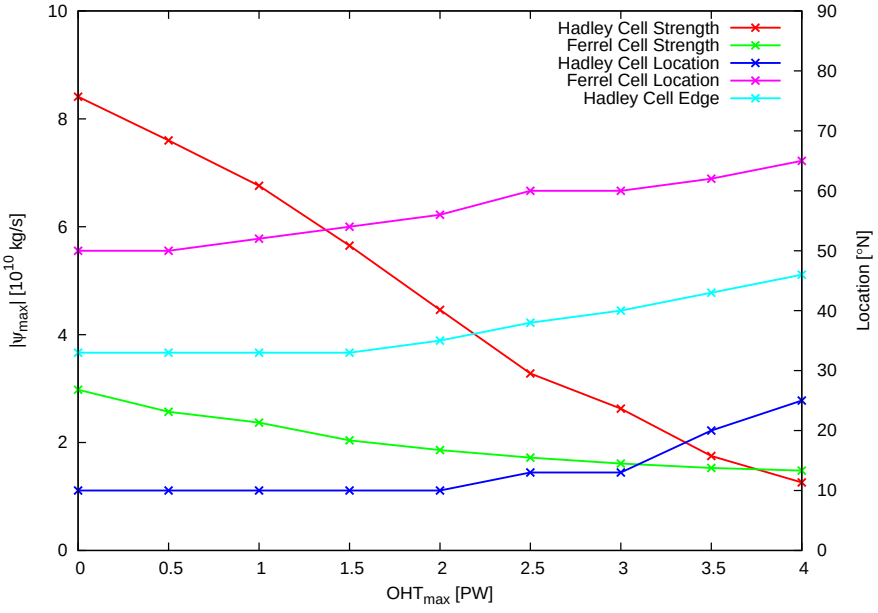

Figure 7. Climatological annual mean mass stream function (Northern Hemisphere): strength (in $10^{10}\,\mathrm{kg\,s^{-1}}$) and location (in $^\circ$ N) of Hadley and Ferrel cell for all simulations.

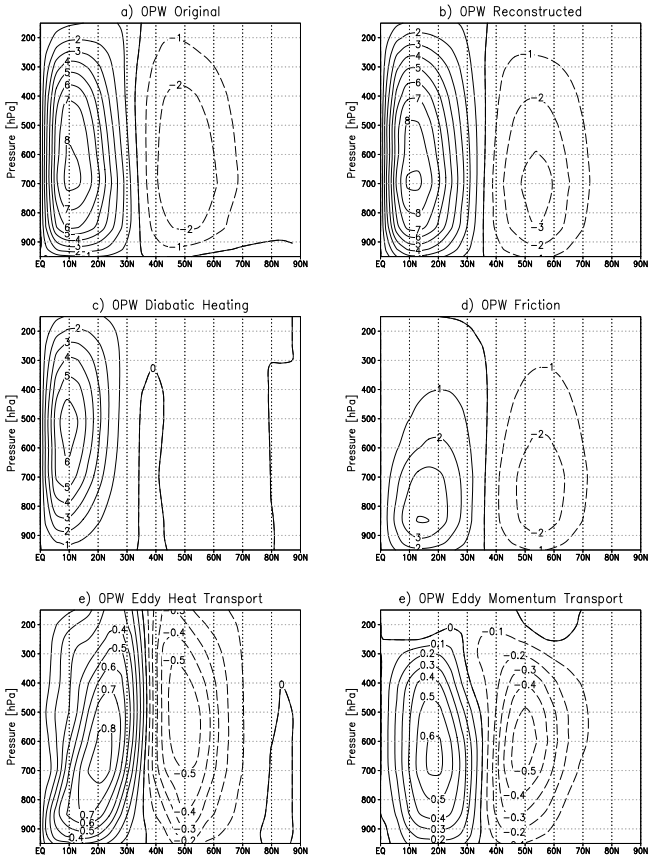

Figure 8. Climatological annual mean mass stream function (in $10^{10}\,\mathrm{kg\,s^{-1}}$) for $\mathrm{OHT_{max}} = 0\,\mathrm{PW}$: **(a)** original (see Fig. 6); **(b)** computed from the Kuo–Eliassen equation (all sources); **(c)** source from diabatic heating; **(d)** source from friction; **(e)** source from eddy heat transport; **(f)** source from eddy momentum transport.

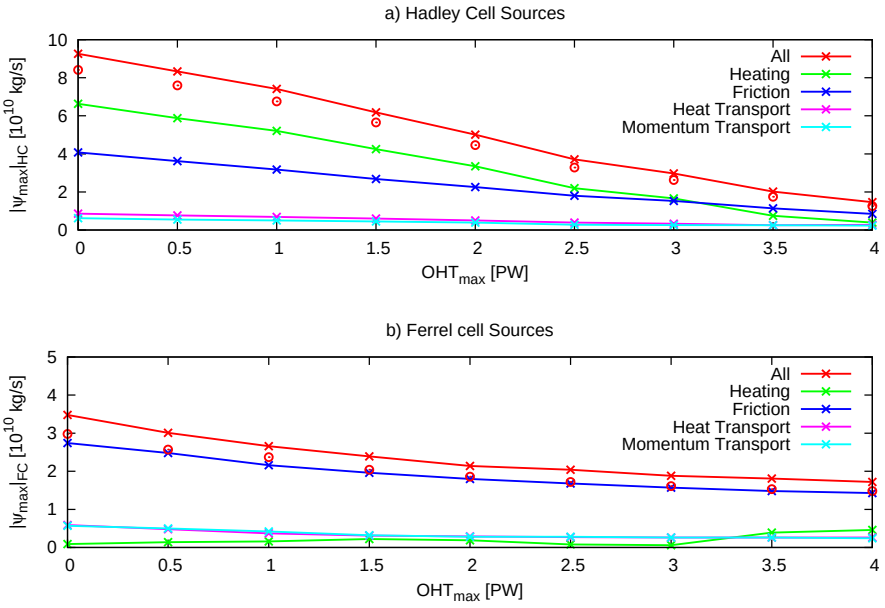

Figure 9. Sources (in $10^{10}\,\mathrm{kg\,s^{-1}}$) of the Hadley (upper) and the Ferrel (lower) cell according to the Kuo–Eliassen equation. Circles indicate the actual strength of the respective cell

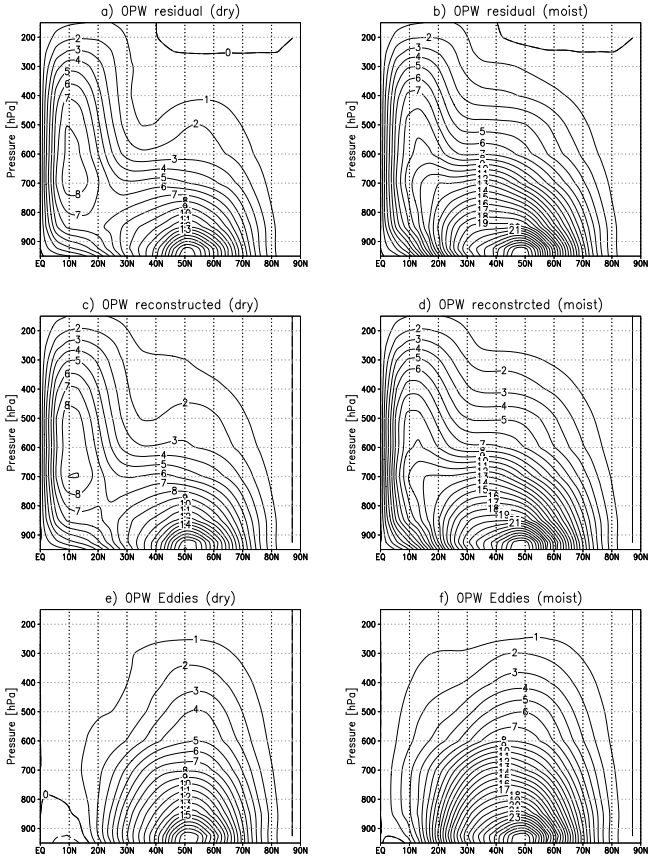

Figure 10. Climatological annual mean residual stream function (in $10^{10}\,\mathrm{kg\,s^{-1}}$) for $\mathrm{OHT_{max}} = 0\,\mathrm{PW}$: **(a)** original dry; **(b)** original moist; **(c)** reconstructed dry; **(d)** reconstructed moist; **(e)** eddy source dry; **(f)** eddy source moist.

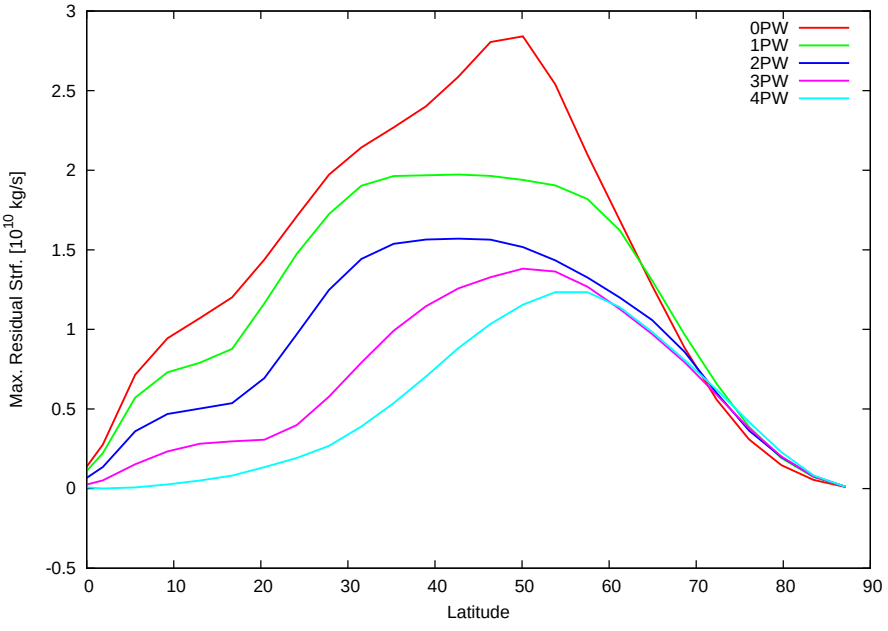

Figure 11. Maximum of moist residual mean stream function (in $10^{10}\,\mathrm{kg\,s^{-1}}$) for $\mathrm{OHT}_{\max} = 0$, 1, 2, 3, and 4 PW.

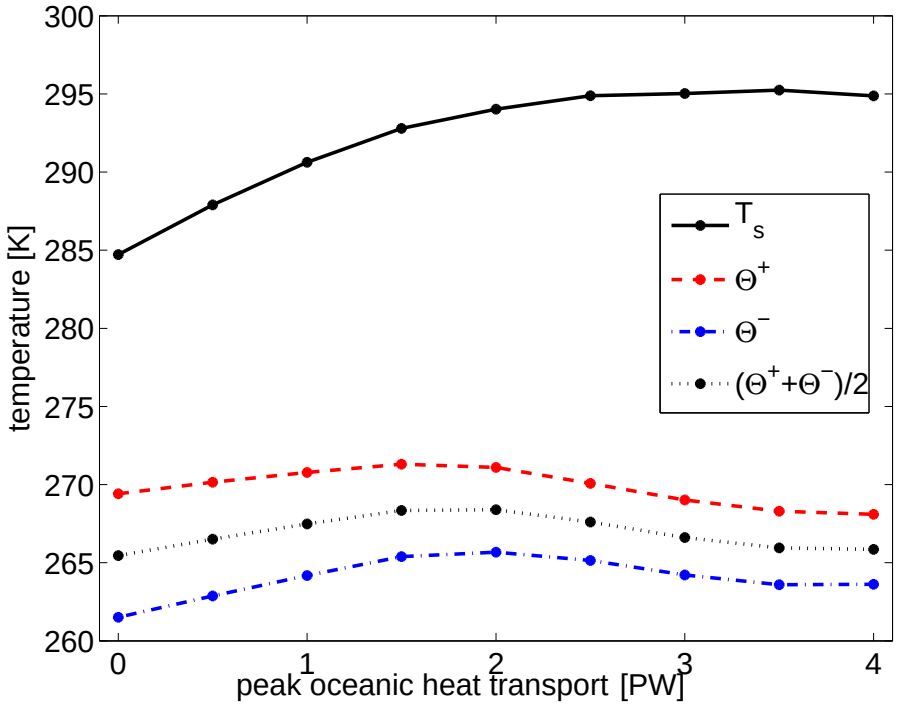

Figure 12. Time average of the global mean surface temperature T_s and of the temperature of the warm (Θ^+) and the cold (Θ^-) pool.

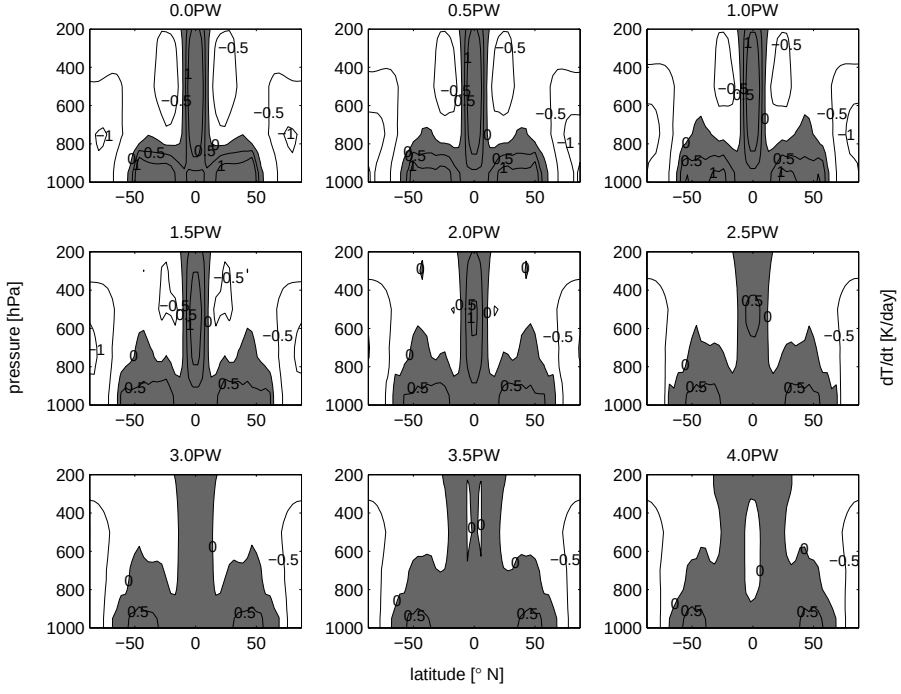

Figure 13. Zonally averaged mean heating rates in the atmosphere for oceanic heat transport ranging from $0.0\,\mathrm{PW}$ (upper left panel) to $4.0\,\mathrm{PW}$ (low right panel), where grey–shaded areas indicate positive and white areas negative heating rates in $[\frac{\mathrm{K}}{\mathrm{day}}]$.

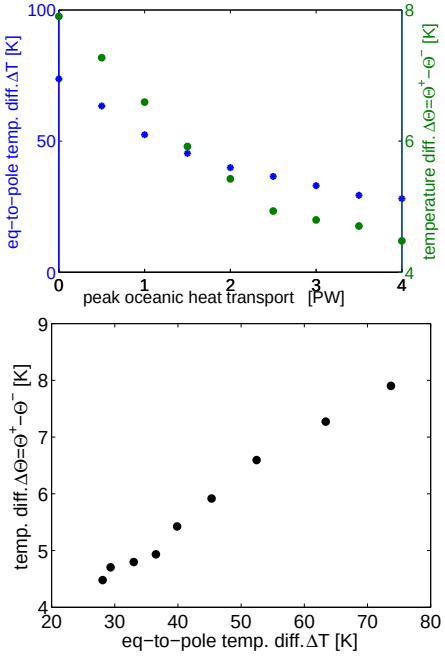

Figure 14. Upper: Scatter plot of time–averaged global mean temperature difference between equator and pole (blue) as well as Θ^+ and Θ^- (green) as a function of maximum energy transport in the ocean. Lower: Scatter plot of time–averaged global mean temperature difference between equator and pole as well as Θ^+ and Θ^-.

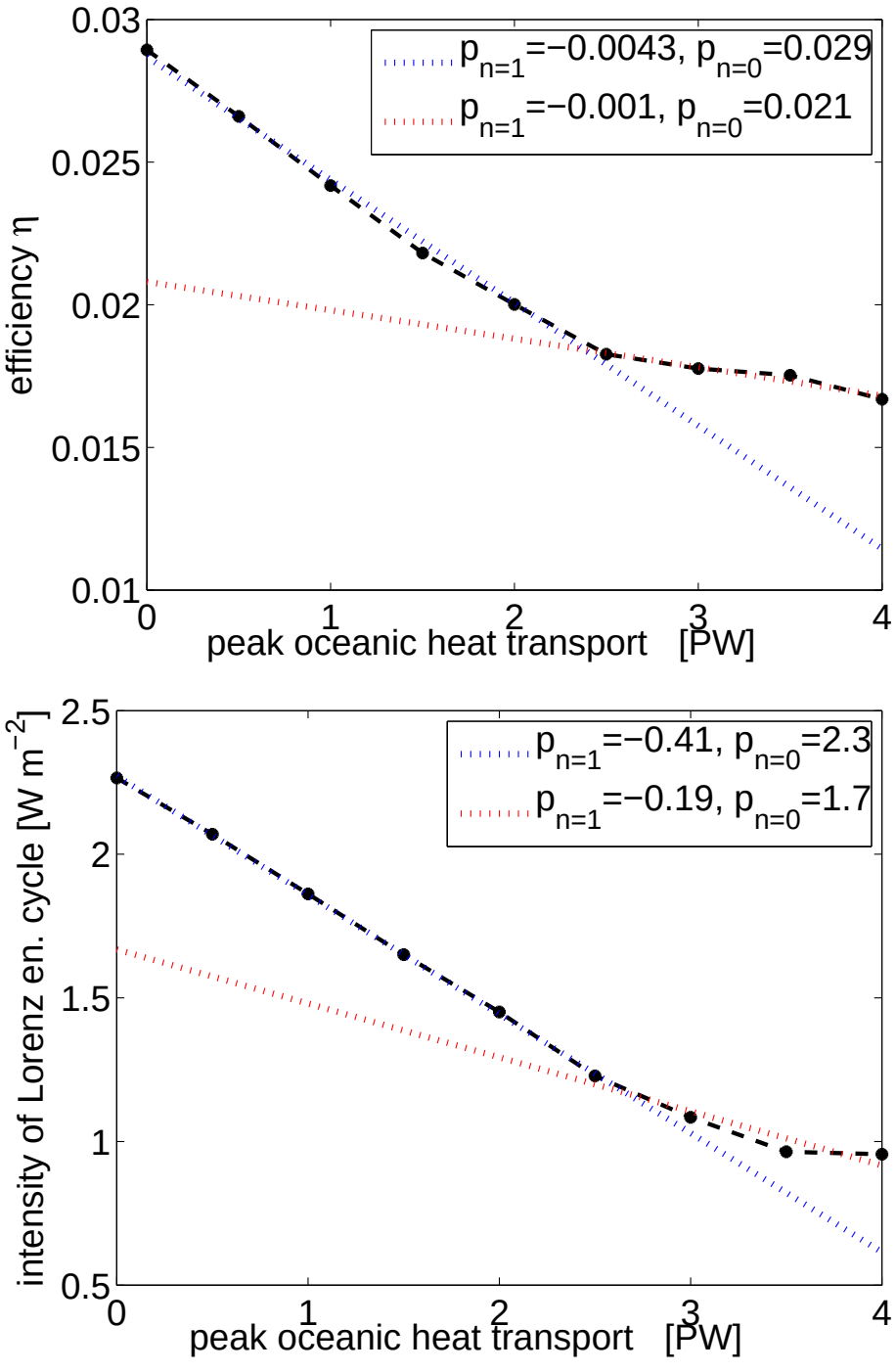

Figure 15. Time average of efficiency η (upper) and intensity of the Lorenz energy cycle $\overline{\dot{W}}$ (lower) for steady state obtained for varying oceanic heat transport. Dotted line represents best linear fit for i) $0.0\,\mathrm{PW} \leq \mathrm{OHT}_{\mathrm{max}} \leq 2.5\,\mathrm{PW}$ (blue)and for ii) $2.5\,\mathrm{PW} \leq \mathrm{OHT}_{\mathrm{max}} \leq 4.0\,\mathrm{PW}$ (red) with polynomial coefficients of n-th order, $\mathrm{p}_{\mathrm{n}=1}$ and $\mathrm{p}_{\mathrm{n}=0}$.

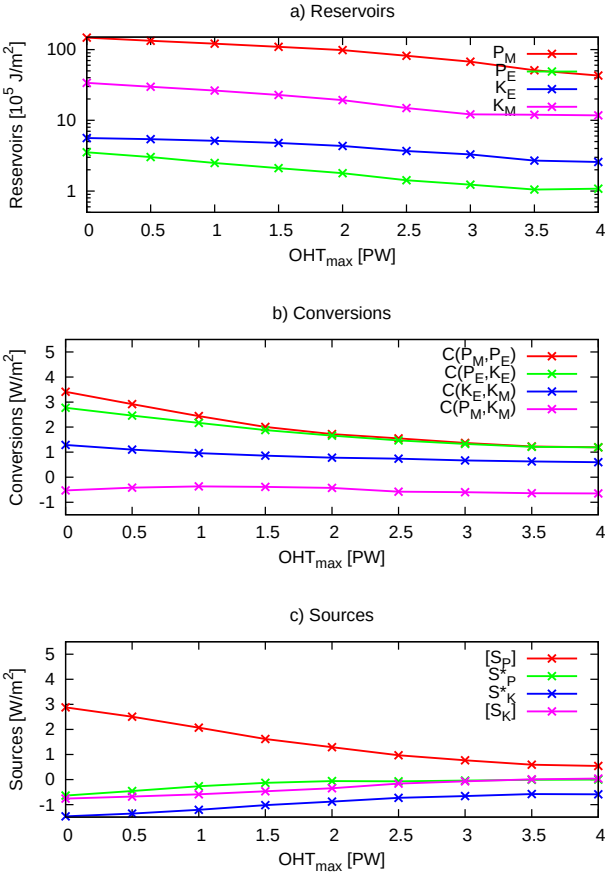

Figure 16. Climatological mean Lorenz energy cycle: reservoirs (upper, in $10^5\,\mathrm{J\,m^{-2}}$), conversions (middle, in $\mathrm{W\,m^{-2}}$) and sources/sinks (lower, in $\mathrm{W\,m^{-2}}$) for all simulations.

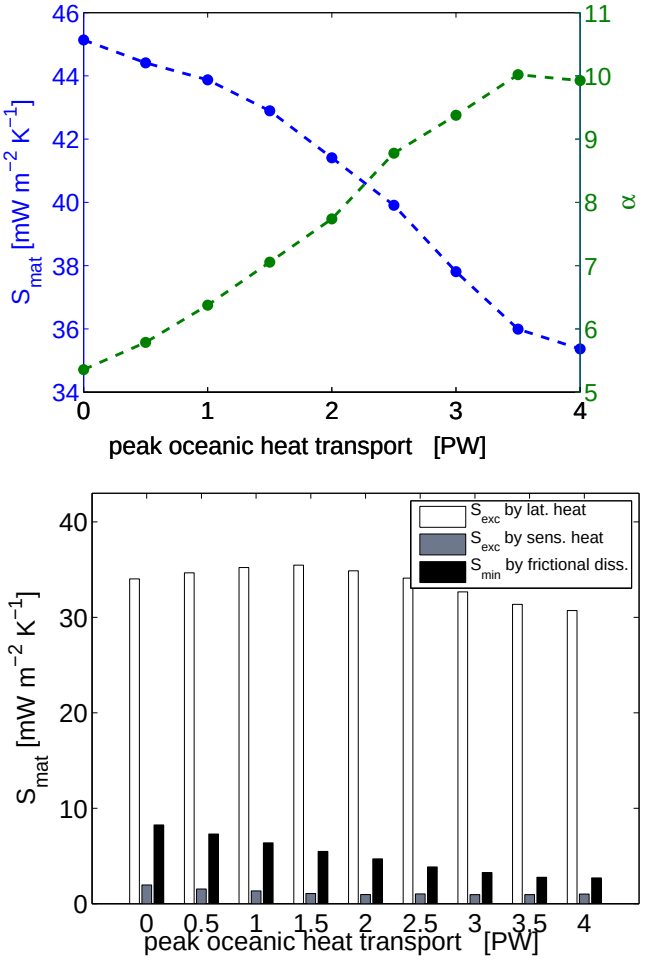

Figure 17. Upper: steady–state global mean material entropy production $\overline{\dot{S}_{mat}}$ (blue graph) and degree of irreversibility α. Lower: most relevant contributions of $\overline{\dot{S}_{mat}}$ split into $\overline{\dot{S}_{exc}}$ and $\overline{\dot{S}_{min}}$, as a function of increasing oceanic heat transport.

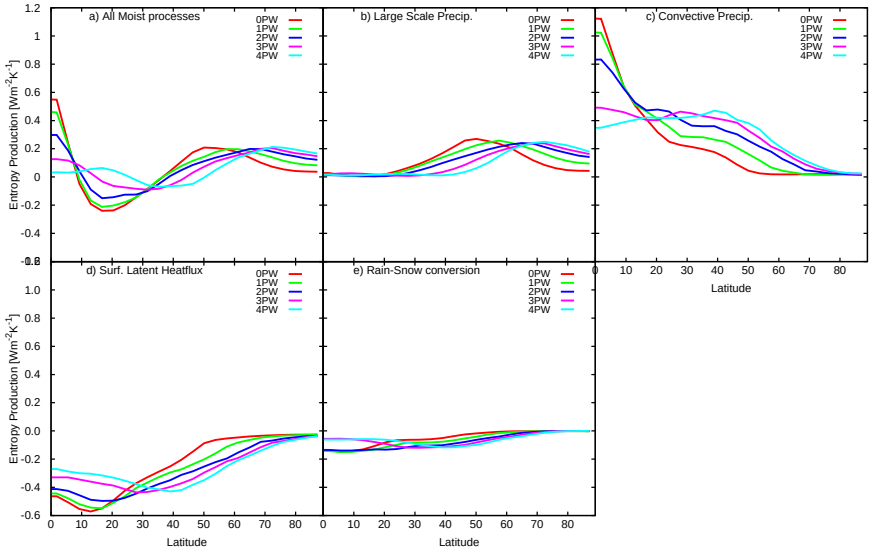

Figure 18. Entropy production from moist processes for $\mathrm{OHT}_{\mathrm{max}} = 0$, 1, 2, 3, and 4 PW.